Materials **2013**, *6*, 4574-4608; doi:10.3390/ma6104574

OPEN ACCESS

materials

ISSN 1996-1944

www.mdpi.com/journal/materials

Review

The Current Status of Hydrogen Storage Alloy Development for Electrochemical Applications

Kwo-hsiung Young * and Jean Nei

BASF/Battery Materials-Ovonic, 2983 Waterview Drive, Rochester Hills, MI 48309, USA;
E-Mail: jean.nei@BASF.com

***** Author to whom correspondence should be addressed; E-Mail: kwo.young@BASF.com; kwoyoung@yahoo.com; Tel.: +1-248-293-7000; Fax: +1-248-299-4228.

Received: 30 August 2013; in revised form: 22 September 2013 / Accepted: 7 October 2013 / Published: 17 October 2013

Abstract: In this review article, the fundamentals of electrochemical reactions involving metal hydrides are explained, followed by a report of recent progress in hydrogen storage alloys for electrochemical applications. The status of various alloy systems, including AB_5, AB_2, A_2B_7-type, Ti-Ni-based, Mg-Ni-based, BCC, and Zr-Ni-based metal hydride alloys, for their most important electrochemical application, the nickel metal hydride battery, is summarized. Other electrochemical applications, such as Ni-hydrogen, fuel cell, Li-ion battery, air-metal hydride, and hybrid battery systems, also have been mentioned.

Keywords: metal hydride; hydrogen storage alloy; NiMH battery; alkaline fuel cell; electrochemical reaction

1. Introduction

Hydrogen storage alloys are important for a few electrochemical applications, especially in the energy storage area. The basic of electrochemical use of the hydrogen storage alloy can be described as follows: when hydrogen enters the lattice of most transition metals, interstitial metal hydride (MH) is formed. The electrons accompanying the hydrogen atoms form a metal-hydrogen band right below the Fermi level, which indicates that the interstitial MH is metallic in nature. While protons in the interstitial MH hop between neighboring occupation sites by quantum mechanical tunneling, the electrons remain within a short distance (3–10 angstroms) of the protons to maintain local charge neutrality. Under the influence of an electric field, electrons and protons will move in opposite

directions. In an electrochemical environment, a voltage is applied to cause electrons to flow, and the charges are balanced out by moving conductive ions through a highly alkaline aqueous electrolyte with good ionic conductivity. During charge, a negative voltage (with respect to the counter electrode) is applied to the metal/metal hydride electrode current collector, and electrons enter the metal through the current collector to neutralize the protons from the splitting of water that occurs at the metal/electrolyte interface (Figure 1a). This electrochemical charging process is characterized by the half reaction:

$$M + H_2O + e^- \rightarrow MH + OH^- \quad (1)$$

During discharge, protons in the MH leave the surface and recombine with OH^- in the alkaline electrolyte to form H_2O, and charge neutrality pushes the electrons out of the MH through the current collector, performing electrical work in the attached circuitry (Figure 1b). The electrochemical discharge process is given by the half reaction:

$$MH + OH^- \rightarrow M + H_2O + e^- \quad (2)$$

Figure 1. Schematics showing the electrochemical reactions between water and metal hydride during charge (**a**) and discharge (**b**). Due to the alkaline nature of the electrolyte, protons cannot desorb or absorb from the surface of metal without the incorporation of water and OH^-.

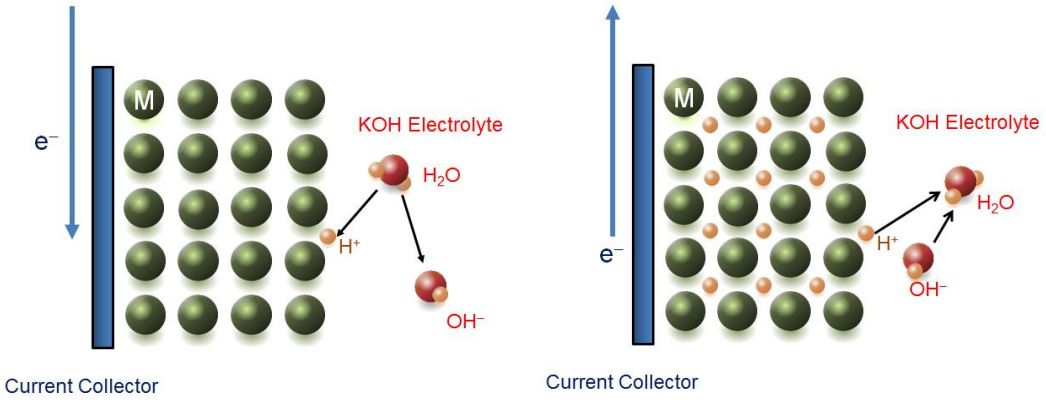

The standard potential of this redox half reaction depends on the chosen MH and is usually as low as possible to maximize the amount of stored energy without exceeding the hydrogen evolution potential (−0.83 V *versus* standard hydrogen electrode). Zn is an exception. With a complete 3d shell, Zn is a natural prohibitor for hydrogen evolution and thus a more negative voltage is possible, which increases the operation voltage of Ni-Zn battery.

The most important electrochemical application for MH is the negative electrode material for nickel metal hydride (NiMH) batteries. Together with a counter electrode from the $Ni(OH)_2$/NiOOH system, which has been used in NiCd and NiFe batteries as early as 1901 by Thomas Edison, the NiMH battery was first demonstrated by researchers in Battelle in 1967 with a mixed TiNi + Ti_2Ni alloy as the negative electrode [1]. Commercialization of the NiMH battery was independently realized by Ovonic Battery Company, Sanyo, and Matsushita in 1989 with AB_2 and AB_5 MH alloys. NiMH battery development started from small cylindrical cells (0.7 to 5 Ah) for portable electronic devices and progressed to 100 Ah prismatic cells for electric vehicle applications. The first commercially available

electric vehicle in the modern era was the EV1 produced by General Motors in 1999. It was powered by a 26.4 kWh NiMH battery pack. Since then, NiMH batteries have powered more than 5 million hybrid electric vehicles made by Toyota, Honda, Ford, and other automakers, demonstrating the robustness and longevity of the NiMH battery. Recently, the NiMH battery has ventured into the stationary application market with advantages in long service life, a wide temperature range, low costs averaged over the service life, abuse immunity, and environmental friendliness. Several reviews on the topic of MH used in NiMH batteries are available [2–10]. In this report, we present the recent progress since the last review made in 2010 [10].

Besides NiMH batteries, MH (most commonly the misch metal-based AB_5 MH alloy) can also be used in other electrochemical applications such as lithium-ion based batteries and metal-air batteries. Metal hydride electrodes have a potential window of 0.1 to 0.5 V *versus* Li+/Li and the lowest polarization among conversion electrodes. These MH electrodes have shown the capability for greater capacity and can be used as anode electrodes in lithium-ion battery [10–12]. An air-MH battery that utilizes a misch metal-based AB_5 alloy in conjunction with a perovskite oxide-based cathode has been demonstrated by several research groups [13–15]. New types of V-flow/NiMH [16,17] and lead-acid/NiMH hybrid batteries [18] have been developed at the University of Hong Kong. Pd-treated $LaNi_{4.7}Al_{0.3}$ has been used in a Ni-hydrogen battery [19]. Another application of $LaNi_5$ is the use as a cathode in a photo-electrochemical cell for water decomposition [20].

2. Hydrogen Storage Alloys for NiMH Battery Negative Electrodes

The use of MH in NiMH batteries started with research conducted by Schmitt and Beccu at Battelle Memorial Institute (TiNi-based) [1,21] and William and Buschow at Philips Research Laboratories ($LaNi_5$-based) [2,22]. Almost 50 years of research on this subject have been conducted. In 2001, nine requirements were established for a suitable MH alloy for NiMH batteries: high capacity, good electrochemical catalysis, easy formation, excellent corrosion resistance, suitable hydrogen equilibrium, good kinetics and efficiency, long cycle life, small pressure-concentration-temperature (PCT) hysteresis, and low cost [6]. Today, the main implementation of NiMH batteries has shifted from consumer portable devices to hybrid electric vehicle and stationary applications. Accordingly, new criteria for suitable MH alloy design requirements, such as low self-discharge, good kinetics at low temperature, fast proton diffusion in the bulk, low pulverization rate during service life, and endurance of high temperature storage, are required for these applications. The amount of metallic inclusions in the MH surface oxide after activation and the high-rate dischargeability (HRD) are characteristics that are essential in meeting many of these new requirements. While the former can be quantified by magnetic susceptibility, the latter is studied by analyzing the surface reaction current density and bulk diffusion constant. Typical values from several alloy systems are compared and listed in Table 1 for reference. Recent progress of MH alloys for NiMH battery applications is reviewed in the following sub-sections categorized by alloy system.

Table 1. Properties comparison of several metal hydride (MH) alloys. Saturated magnetic susceptibility (M_S) is proportional to the total amount of metallic nickel in the surface after activation. Applied magnetic field corresponding to half of the saturated magnetic susceptibility ($H_{1/2}$) is inversely proportional to the average number of Ni atoms in a cluster. Surface exchange current (I_0) and diffusion constant (D) are qualitative measurements of the catalytic nature of the surface reaction and the proton transportation in the bulk of the alloy, respectively.

Alloy system	Composition	M_S (memu g^{-1})	$H_{1/2}$ (kOe)	I_0 (mA g^{-1})	D (×10^{-11} cm^2 s^{-1})	Reference
AB_2	$Ti_{12}Zr_{21.5}Ni_{36.2}V_{9.5}Cr_{4.5}Mn_{13.6}Sn_{0.3}Co_2Al_{0.4}$	33	0.162	32.1	9.7	[23]
AB_5	$La_{10.5}Ce_{4.3}Pr_{0.5}Nd_{1.4}Ni_{60.0}Co_{12.7}Mn_{5.9}Al_{4.7}$	434	0.173	43.2	25.5	[23]
A_2B_7	$La_{16.3}Mg_{7.0}Ni_{65.1}Co_{11.6}$	369	0.125	41.0	30.8	[23]
A_2B_7	$Nd_{18.8}Mg_{2.5}Ni_{65.1}Al_{13.6}$	132	0.171	22.7	11.4	[23]
A_2B_7	$La_{3.8}Pr_{7.7}Nd_{7.7}Mg_{4.0}Ni_{72.1}Al_{4.7}$	314	0.128	51.5	31.9	This work
A_2B_7	$Nd_{18.4}Zr_{0.2}Mg_{3.6}Ni_{74.1}Co_{0.1}Al_{3.5}$	679	0.102	52.5	64	[24]
Zr-A_2B_7	Zr_2Ni_7	213	0.281	22.3	41	This work, [25]
Zr-AB_5	$ZrNi_{4.5}$	2286	0.400	20.1	60.6	This work, [26]

2.1. Rare Earth-Based AB_5 Alloys

Vucht *et al.* first reported the hydrogen storage capability of rare earth-based AB_5 intermetallic alloy in 1970 [27]. Since then, this alloy system has become the most widely used intermetallic alloy in all metal hydride applications. After over 40 years of research, many compositions, structures, processes, and electrode fabrication modifications have been performed. Recent efforts have focused on (1) cost reduction by introducing Fe and Cu into the alloy formula to reduce/eliminate expensive Co and (2) improvement in HRD and low-temperature performance. The effects of substituting Ni by Cu, Fe, and Mo on charge-transfer resistance at −40 ℃ are summarized in Figure 2. The unit of Ω·g for charge-transfer resistance is used instead of the traditionally used Ω to rid the contribution from amount of electrode material; therefore, the values can be compared fairly among various MH alloys. The effect of Fe on charge-transfer resistance performance is interesting and can be explained by the evolutions of two factors: surface reaction area and catalytic ability. While surface catalytic ability is increased monotonically as the level of Fe-addition increases, surface reaction area is increased by 1% of Fe but decreased by further addition [28]. Consequently, charge-transfer resistance decreases with 1% Fe due to the improvements in both surface reaction area and catalytic ability, increases with a little higher Fe-content as the surface area diminishes, and finally decreases (but not to the level achieved with 1% Fe) with high amount of Fe when the surface catalytic ability takes on a more dominating role. Other research works on AB_5 alloys are summarized in Table 2.

Table 2. Summary of recent research on misch metal-based AB_5 MH alloys. S: substitution, P: process, A: additives.

Method	Alloy formula/process/additives	Secondary phase (s)	Range of *x*, *etc.*	Capacity	HRD	Cycle life	Charge retention	Low temperature	Reference
S	$La_{10.5}Ce_{4.3}Pr_{0.5}Nd_{1.4}Ni_{64.3-x}$ $Co_{5.0}$ $Mn_{4.6}Al_{6.0}Zr_{0.2}Fe_x$	–	0 to 1.5	down	up	down	down	up	[28]
S	$La_{10.5}Ce_{4.3}Pr_{0.5}Nd_{1.4}Ni_{64.3}Co_{8.4-x}Mn_{4.6}Al_{6.0}Cu_x$	(Al, Mn)Ni	0 to 5.4	down	up	down	up	up	[29]
S	$La_{10.5}Ce_{4.3}Pr_{0.5}Nd_{1.4}Ni_{64.3-x}$ $Co_{5.0}$ $Mn_{4.6}Al_{6.0}Zr_{0.2}Mo_x$	Mo	0 to 4	down	down	same	same	up	[30]
S	$La_{10.5}Ce_{4.3}Pr_{0.5}Nd_{1.3}Ni_{67.7-x-y}Mn_xAl_y$	–	Mn (0–0.6), Al (0–3.4)	–	–	up	up	–	[31]
S	$NdNi_{5-x-y-z}Co_xAl_yMn_z$	–	Co (0–0.5), Al (0–0.5), Mn (0–0.8)	up	down	up	down	–	[32]
S	$La_{0.7}Ce_{0.3}Ni_{3.75}Mn_{0.35}$ $Al_{0.15}Cu_{0.75-x}Fe_x$	–	0 to 0.2	down	down	up	–	–	[33]
S	$La_{0.7}Ce_{0.3}Ni_{3.85}Mn_{0.8}Cu_{0.4}$ $Fe_{0.15-x}(Fe_{0.43}B_{0.57})_x$	$La_3Ni_{12}B_2$	0 to 0.15	down	up	down	–	–	[34]
S	$LaNi_{3.55}Co_{0.2-x}Mn_{0.35}Al_{0.15}$ $Cu_{0.75}(Fe_{0.43}B_{0.57})_x$	$La_3Ni_{12}B_2$	0 to 0.1	down	up	down	–	–	[35]
S	$LaNi_{3.55}Co_{0.2-x}Mn_{0.35}Al_{0.15}Cu_{0.75}(V_{0.81}Fe_{0.19})_x$	Ni-rich, La-rich	0 to 0.05	up	up	down	–	–	[36]
S	$La_{0.7}Ce_{0.3}Ni_{3.75-x}Mn_{0.35}Al_{0.15}Cu_{0.75}(Fe_{0.43}B_{0.57})_x$	–	0 to 0.15	up	up	up	–	–	[37]
S	$La_{0.7}Ce_{0.3}Ni_{3.83-x}Mn_{0.35}Al_{0.15}Cu_{0.75}(Fe_{0.43}B_{0.57})_x$	$La_3Ni_{12}B_2$	0 to 0.15	down	up	down	–	–	[38]
S	$La_{0.7}Ce_{0.3}Ni_{3.75-x}Mn_{0.35}Al_{0.15}Cu_{0.75}(V_{0.81}Fe_{0.19})_x$	–	0 to 0.05	down	up	up	–	–	[39]
S	$La_{0.7}Ce_{0.3}Ni_{4.2}Mn_{0.9-x}Cu_{0.37}(V_{0.81}Fe_{0.19})_x$	(V, Mn, Ni)	0 to 0.1	same	up	down	–	–	[40]
S	$La_{0.7}Ce_{0.3}Ni_{4.2}Mn_{0.9-x}Cu_{0.37}(Fe_{0.43}B_{0.57})_x$	$La_3Ni_{12}B_2$	0 to 0.1	down	up	down	–	–	[41]
S	$La_{0.7}Ce_{0.3}Ni_{3.75}Mn_{0.35}Al_{0.15}Cu_{0.75-x}(Fe_{0.43}B_{0.57})_x$	$La_3Ni_{12}B_2$	0 to 0.1	down	up	up	–	–	[42]
S	$La_{0.7}Ce_{0.3}Ni_{3.75}Mn_{0.35}Al_{0.15}Cu_{0.75-x}(V_{0.81}Fe_{0.19})_x$	–	0 to 0.1	same	up	up	–	–	[43]
S	$La_{0.7}Ce_{0.3}(Ni_{3.65}Mn_{0.35}Al_{0.15}Cu_{0.75}(Fe_{0.43}B_{0.57})_{0.10})_x$	$La_3Ni_{12}B_2Ce_2Ni_7$	0.9 to 1.0	up	up	up	–	–	[44]
S	$MlNi_{3.55}Co_{0.75-x}Mn_{0.4}Al_{0.3}(Cu_{0.75}P_{0.25})_x$	P-rich, Mn-rich	0 to 0.5	down	up	up then down	–	–	[45,46]
S	$LaNi_{5-x}In_x$	–	0.1 to 0.5	down	–	up	–	–	[47]
S	$LaNi_{4.3}(Co,Al)_{0.7-x}In_x$	–	0 to 0.1	up	up	–	–	–	[48]
S	$LaNi_{4.1-x}Co_{0.6}Mn_{0.3}Al_x$	–	0 to 0.45	down	down	up	up	–	[49]
S	$La_{0.78}Ce_{0.22}Ni_{3.73}Mn_{0.30}Al_{0.17}Fe_xCo_{0.8-x}$	–	0 to 0.8	down	down	up	up	–	[50]
S	$LaNi_{4.4-x}Co_{0.3}Mn_{0.3}Al_x$	–	0 to 0.2	up	Up then down	up	up	–	[51]
S	$MmNi_{3.70-x}Mn_{0.35}Co_{0.60}Al_{0.25}B_x$	$CeCo_4B$	0 to 0.2	down	up	–	–	–	[52]
S	$La_{0.35}Ce_{0.65}Ni_{3.54}Mn_{0.35}Co_{0.80-x}Al_{0.32}Mo_x$	–	0 to 0.25	up	up	up	–	–	[53]
S	$Mm_{0.8-x}Ti_xLa_{0.2}Ni_{3.7}Mn_{0.5}Co_{0.3}Al_{0.38}Mo_{0.02}$	–	0 to 0.05	up	–	up	up	–	[54]
S	$La_{0.65-x}Ce_{0.25-x}Pr_{0.03}Nd_{0.07}Y_{2x}Ni_{3.65}Mn_{0.3}Co_{0.75}Al_{0.3}$	–	0 to 0.04	down	down	up	–	–	[55]
S	$La_{1-x}Y_xNi_{3.55}Mn_{0.4}Co_{0.75}Al_{0.3}$	–	0 to 0.1	up	–	up	–	–	[56]

Table 2. *Cont.*

Method	Alloy formula/process/additives	Secondary phase (s)	Range of *x*, *etc.*	Capacity	HRD	Cycle life	Charge retention	Low temperature	Reference
S	Eliminates Co, Mn	–	–	up	–	–	up	–	[57]
P	Pre-treatment if 12 M NaOH + 0.05 M $NaBH_4$	–	–	–	up	up	–	up	[58]
P	Melt-spin	$LaNi_3$, La_2Ni_3	–	up	–	down	–	–	[59]
P	Gas Atomization	–	–	down	same	up	up	same	[29]
P	Annealing temperature increase	–	–	up	down	up	up	–	[60]
A	Ni-PTFE plating	–	–	same	–	potentially up	–	–	[61]
A	Carbon nanosphere	–	–	up	up	down	–	–	[62]
A	Graphite	–	–	down	up		–	–	[63]
A	Co nano and Y_2O_3	–	–			up	–	–	[64]
A	Co_3O_4	–	–	up	up		–	–	[65]
A	Co_3O_4	–	–	up	up	up	–	–	[66]
A	$Ni(OH)_2$	–	–	up	up	down	–	–	[67]

Figure 2. Plot of charge-transfer resistance measured at −40 ℃ by AC impedance as a function of Fe-, Mo-, or Cu-substitution in AB_5 MH alloy [28–30]. All three additives at the lowest substitution level contribute positively in lowering the resistance.

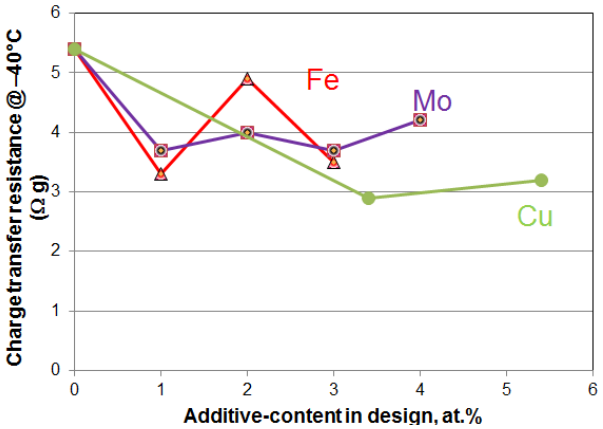

2.2. Laves Phase-Based AB_2 Alloys

AB_2 alloys for NiMH battery applications are composed of main phases belonging to a family of materials known as Laves phases: hexagonal C14 phase and face-center-cubic C15 phase. C36 phase may also be present but is difficult to distinguish from C14 in XRD analysis. The main controlling factor for the C14/C15 ratio is the average electron density (*e*/*a*). Nei *et al.* reported that chemical potential can be used to fine-tune the C14/C15 threshold when Ti, Zr, and Hf, which have the same number of outer-shell electrons, are used together [68]. The common minor phases are Zr_7Ni_{10}, Zr_9Ni_{11}, ZrNi, and TiNi. The microstructures [69–72] and the contributions [73–77] of these phases were studied extensively in recent years.

While many studies on AB_2 alloys were reported, most of them focused on the influences of A- or B-site substitutions on electrochemical properties. These results are summarized in Table 3. The effect of partial substitution of Ni by various modifiers on −40 ℃ charge transfer resistance is summarized in Figure 3.

As shown in Figure 3, both La and Si are very effective in improving the low-temperature performance. Additionally, the influence of stoichiometry (B/A ratio) on electrochemical properties was reported [78,79]. PCT hysteresis was correlated to the pulverization rate in AB_2 alloys [80–82]. Gas atomization and hydrogen annealing were introduced to produce AB_2 metal powder directly [83,84]. V-free AB_2 alloys were also developed to reduce raw material costs [85,86].

Table 3. Summary of recent research on Laves phase-based AB_2 MH alloys.

Base alloy	Substitution	Major effects	Reference
C14-domintaed	Al	Al improves bulk diffusion and surface reactivity. Al and Co together improves all electrochemical performances	[87,88]
C14-domintaed	B	B improves HRD and low-temperature performance but decreases charge retention, capacity, and cycle life	[85]
C14-domintaed	C	C increases HRD and charge retention but decreases low-temperature, capacity and cycle life	[85]
C14-domintaed	Co	Co provides easy activation, improves/decreases capacity, better cycle life and charge retention, but impedes HRD	[87,89,90]

Table 3. *Cont.*

Base alloy	Substitution	Major effects	Reference
C14-domintaed	Cr	Cr improves charge retention but impedes HRD	[89]
C14-domintaed	Mo	Mo improves HRD, low-temperature performance, charge retention, and cycle life	[91]
C14-domintaed	Cu	Cu increases capacity, facilitates activation, but decreases HRD.	[92]
C14-domintaed	Fe	Fe facilitates activation, increases total electrochemical capacity and effective surface reaction area, decreases HRD and bulk diffusion, and deteriorates low-temperature performance	[87,93]
C14-domintaed	Gd	Gd improves low-temperature performance, but decreases charge retention, HRD, capacity, and cycle life	[85]
C14-domintaed	La	La improves capacity, HRD, and low-temperature performance with a trade-off of inferior cycle stability	[94]
C14-domintaed	Mg	Mg improves charge retention, deteriorates capacity, low-temperature performance, and cycle life	[85]
C14-domintaed	Mn	Mn increases capacity, facilitates activation, but decreases cycle life	[89,95]
C14-domintaed	Ni	Ni improves cycle life and HRD but reduces capacity	[89]
C14-domintaed	Pt	Pt improves capacity and HRD	[96]
C14-domintaed	Si	1 at % of Si is beneficial to HRD and low-temperature performance	[97]
C14-domintaed	Sn	Sn improves charge retention but deteriorates HRD and cycle life	[87,98]
C14-domintaed	Ti	Ti increases HRD and facilitates activation	[99]
C14-domintaed	V	V increases capacity but decreases HRD and charge retention	[100]
Both C14- and C15-dominated	Y	Y improves activation, HRD, and low-temperature performance by increasing reaction surface area	[101,102]
C14-domintaed	Zr	Zr increases capacity	[99]

Figure 3. Plot of charge-transfer resistance measured at −40 ℃ by AC impedance as function of Cu-, Fe-, Y-, Mo-, La-, or Si-substitution in AB_2 MH alloy [91–94,97,102]. La- and Si-modified alloys demonstrate the lowest resistance.

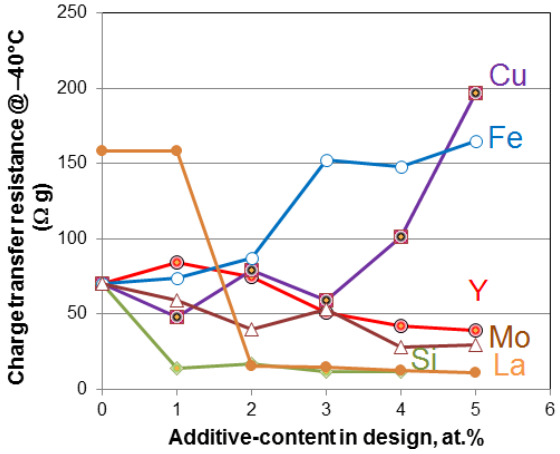

2.3. Superlattice A_2B_7-Type (A_2B_4-AB_5-Hybrid-Type, such as AB_3, A_2B_7, A_5B_{19}, and AB_4) Alloys

Mg-containing superlattice alloys have been used extensively in Japanese-made NiMH batteries for retail market since the introduction by Sanyo (eneloop) [103–105]. Batteries with superlattice A_2B_7-type alloys as negative electrode exhibit much lower self-discharge compared to ones with traditionally used AB_5 alloys [105]. Therefore, NiMH battery's storing and ready-to-use-out-of-the-pack

capabilities can be much improved by the use of superlattice alloy, which enable NiMH battery to grow much more competitive compared to primary battery. Furthermore, superlattice alloys have been reported to have superior capacity, cycle life, and high-rate performances compared to the conventional alloys and are becoming a dominating force in both consumer and hybrid electric vehicle markets. The multi-phase MH system, with an overall B/A ratio between 3 and 4, is composed of a number of AB_5 slabs placed between two A_2B_4 slabs (Figure 4). Mg is needed to lower the average metal-hydrogen bond strength in order to obtain the appropriate heat of hydride formation suitable for NiMH battery applications (≈ −39 kJ mol^{-1} H_2 at room temperature and 1 atm), and its replacement amount for rare earth is about 30% and 15% for La and Nd, respectively. Mg mainly replaces rare earth elements on the A_2B_4 slab. The distribution of Mg (which has a high vapor pressure during melting) in the alloy is particularly important because Mg-lean regions have a tendency to form AB_5 phase. Lin *et al.* presented a brief review of different types of A_2B_7 alloys [106]. The superlattice MH alloys can be classified into three groups: La-only, La-Pr-Nd, and Nd-only. The addition of Ce promotes AB_5 phase and therefore is rarely used. The La-only group has the highest capacity but the shortest cycle life due to the easy oxidation of La. The Nd-only group has the best charge retention and cycle life performance but the lowest capacity. Properties of the La-Pr-Nd group fall between the properties for La- and Nd-only alloys. Annealing is the most convenient method to manipulate phase distribution, and its effect was reported on La-only [107–113], Nd-only [24], La-Gd [114], La-Nd [115], La-Pr-Nd [116,117], and La-Ce-Pr-Nd [118] alloys. While Nd-only and La-Pr-Nd superlattice alloys are used in low self-discharge and high capacity NiMH batteries, respectively, La-only superlattice alloy is not used in commercial products due to its low cycle life from pulverization [119]. However, La-only alloy is studied extensively in the research society [120] due to easy sample preparation. The recent progress in the NiMH battery applications of superlattice alloys is summarized in Table 4.

Figure 4. Schematics of stacking sequences of superlattice alloy systems. The stacking sequence is constructed with one to four AB_5 (blue 15) slabs in between slabs of A_2B_4 (red 24). Two structures are available for each stacking sequence depending on the direction of the A_2B_4 slab shifts. The tilted stacking of A_2B_4 in a C14 structure first shifts (1/3, 1/3) and then shifts back (−1/3, −1/3) while C15 structure shifts (1/3, 1/3) consecutively on the *a*-*b* plane.

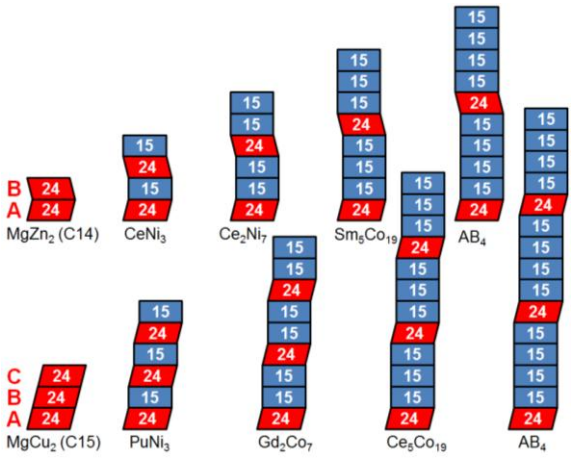

Table 4. Summary of recent progress in electrochemical property improvement in superlattice MH alloys.

Substitution/Process	Alloy formula	Range of *x*	Capacity	HRD	Cycle life	Charge retention	Comment	Reference
Ce	$(La_{0.7}Mg_{0.3})_{1-x}Ce_xNi_{2.8}Co_{0.5}$	0 to 0.1	down	up	up	–	–	[121]
Dy	$(La_{1-x}Dy_x)_{0.8}Mg_{0.2}Ni_{3.4}Al_{0.1}$	0 to 0.2	up	–	same	down	–	[122]
Gd	$(La_{2-x}Gd_xMg)(NiCoAlZn)_{3.5}$	0 to 1	up	down	up	–	–	[123]
Nd	$La_{0.8-x}Nd_xMg_{0.2}Ni_{3.35}Al_{0.1}Si_{0.05}$	0 to 0.2	up	up	up	–	–	[124]
Nd	$(La_{1-x}Nd_x)_2Mg(Ni_{0.8}Co_{0.15}Mn_{0.05})_9$	0 to 0.3	down	–	up	–	–	[125]
Pr	$La_{0.75-x}Pr_xMg_{0.25}Ni_{3.2}Co_{0.2}Al_{0.1}$	0 to 0.4	–	–	up	–	–	[126]
Pr	$La_{0.8-x}Pr_xMg_{0.2}Ni_{3.15}Co_{0.2}Al_{0.1}Si_{0.05}$	0 to 0.3	up	up	up	–	–	[127]
Pr	$La_{0.75-x}Pr_xMg_{0.25}Ni_{3.2}Co_{0.2}Al_{0.1}$	0 to 0.2	down	–	up	–	–	[128]
Sc	$(La_{2-x}Gd_xMg)(NiCoAlZn)_{3.5}$	0 to 1	up	up	same	–	–	[123]
Sm	$La_{0.8-x}Sm_xMg_{0.2}Ni_{3.15}Co_{0.2}Al_{0.1}Si_{0.05}$	0 to 0.1	up	up	up	–	–	[129]
Ti	$(La_{0.67}Mg_{0.33})_{1-x}Ti_xNi_{2.75}Co_{0.25}$	0 to 0.05	down	up	up	–	–	[130]
Ti	$(La_{1-x}Ti_x)_2MgNi_{8.25}Co_{0.75}$	0 to 0.1	down	up	up	–	–	[131]
Zr	$La_{0.75-x}Pr_xMg_{0.25}Ni_{3.2}Co_{0.2}Al_{0.1}$	0 to 0.2	up	–	up	–	–	[128]
Zr	$La_{0.75-x}Zr_xMg_{0.25}Ni_{3.2}Co_{0.2}Al_{0.1}$	0 to 0.2	–	down	–	–	–	[132]
Mg	$La_{1.7+x}Mg_{1.3-x}(NiCoMn)_{9.3}$	0 to 0.4	up	down	down	–	Improves activation	[133]
Mg	$La_{0.85}Pr_{0.15}Mg_x(Ni_{0.7}Co_{0.2}Mn_{0.1})_9$	0.5 to 1.0	up	up	–	–	–	[134]
Mg	$La_{0.8-x}Gd_{0.2}Mg_xNi_{3.1}Co_{0.3}Al_{0.1}$	0.1 to 0.15	up	–	up	–	–	[135]
Mg	$La_{0.8-x}Gd_{0.2}Mg_xNi_{3.1}Co_{0.3}Al_{0.1}$	0 to 0.15	up	–	up	–	–	[136]
Mg	$La_{0.8-x}Gd_{0.2}Mg_xNi_{3.3}Co_{0.3}Al_{0.1}$	0 to 0.15	up	up	up	–	–	[137]
Ca	$La_{0.67}Mg_{0.33-x}Ca_xNi_{2.75}Co_{0.25}$	0 to 0.05	–	up	up	–	–	[138]
Al	$La_{0.75}Mg_{0.25}Ni_{3.5-x}Co_{0.2}Al_x$	0 to 0.09	down	down	up	–	–	[139]
Co	$LaNi_{3.2-x}Mn_{0.3}Co_x$	0.2 to 0.8	down	–	up	up	–	[140]
Co	$La_{0.7}Zr_{0.1}Mg_{0.2}Ni_{3.4-x}Co_xFe_{0.1}$	0.15 to 0.25	down	up	up	–	–	[141]
Co	$La_{0.55}Pr_{0.05}Nd_{0.15}Mg_{0.25}Ni_{3.5-x}Co_xAl_{0.25}$	0 to 0.3	up	up	same	–	–	[142]
Co + Al	$La_{0.45}Pr_{0.135}Nd_{0.315}Mg_{0.1}Ni_{3.9}Al_{0.2}$	0 to 0.1	down	up	up	–	–	[143]
Co + Al	$La_2MgMn_{0.3}Ni_{8.7-x}(Co_{0.5}Al_{0.5})_x$	0 to 2	down	up	up	–	–	[144]
Co + Al	$La_{0.55}Pr_{0.05}Nd_{0.15}Mg_{0.25}Ni_{3.5}(Co_{0.5}Al_{0.5})_x$	0 to 0.3	up	–	up	up	–	[145]
Al	$LaNi_{3.\,8-x}Al_x$	0 to 0.4	up then down	–	–	–	Improves activation	[146]

Table 4. *Cont.*

Substitution/Process	Alloy formula	Range of *x*	Capacity	HRD	Cycle life	Charge retention	Comment	Reference
Mn	$(La_{0.8}Nd_{0.2})_2Mg(Ni_{0.9-x}\ Co_{0.1}Mn_x)_9$	0 to 0.1	up	–	up	–	–	[147]
Mn	$La_{0.78}Mg_{0.22}(Ni_{0.9-x}\ Co_{0.1}Mn_x)_3$	0 to 0.01	down	up	down	–	–	[148]
Cu	$LaMg_2Ni_{9-x}Cu_x$	0 to 9	down	–	–	–	–	[149]
Si	$La_{0.8}Mg_{0.2}Ni_{3.3}Co_{0.52}Si_x$	0 to 0.1	down	up	up	–	–	[107]
Ni	$CeMn_{0.25}Al_{0.25}Ni_{1.5+x}$	0 to 1.1	up	–	–	–	–	[150]
H_2O_2 in electrolyte	$Nd_{18.8}Mg_{2.5}Ni_{75.1}Al_{3.6}$	–	up		up	up	–	[151]
Melt-spin	$La_{0.75-x}Zr_xMg_{0.25}Ni_{3.2}Co_{0.2}Al_{0.1}$	0 to 0.2	–	up	–	–	–	[132]
Melt-spin	La_2MgNi_9	–	–	–	–	–	Improves Mg-homogeneity	[152]
Ball milling	$La_{0.7}Mg_{0.3}Ni_{2.8}Co_{0.5-x}Fe_x$	0 to 0.5	up	–	up	–	–	[153]
NiCuP plating	$La_{0.88}Mg_{0.12}Ni_{2.95}Mn_{0.10}Co_{0.55}Al_{0.10}$	–	up	up	–	up	–	[154]
Spark plasma sintering	$La_{0.85}Mg_{0.15}Ni_{3.8}$	–	same	–	up	–	–	[155]
Polyaniline plating	$La_{0.8}Mg_{0.2}Ni_{2.7}Mn_{0.1}Co_{0.55}Al_{0.1}$	–	–	up	up	–	–	[156]
Magnetic annealing	$La_{0.67}Mg_{0.33}Ni_{3.0}$	–	up	up	up	–	–	[157]
Chemical coprecipitation + metal reduction-diffusion	$La_{0.67}Mg_{0.33}Ni_{3.0}$	–	–	–	–	–	Produces multi-phase structure	[158]

2.4. Ti-Ni-Based Alloys

The Ti-Ni-based system was the first MH alloy used in NiMH batteries in the early 1970 s. Although its development was interrupted by the fast growth of AB_5 alloy, the Ti-Ni system remains a popular research topic due to its low cost, high hydrogen storage capacity, and fast activation. Two types of Ti-Ni binary alloys, TiNi and Ti_2Ni, are able to absorb large amounts of hydrogen and are candidates as negative electrode material in NiMH batteries. TiNi alloy exhibits polymorphism, which is the basis of its outstanding shape memory property that is fully utilized in many industrial applications. Upon cooling, TiNi transforms from a B2 cubic structure (austenite) to a B19' monoclinic structure (martensite). Early electrochemical studies on TiNi alloy demonstrated great activation performance and an electrochemical discharge capacity of 210 to 250 mAh g^{-1} [159,160]. Compared to TiNi, Ti_2Ni MH alloy had higher hydrogen storage capacity due to its higher content of hydride forming Ti in the formulation, but its electrochemical capacity was only 170 mAh g^{-1} with its stronger metal-hydrogen bond strength, an indicator of dehydriding difficulty [160]. By combining TiNi and Ti_2Ni phases, the electrochemical capacity increases up to 320 mAh g^{-1} [160,161] with the assistance of synergetic effect between the two phases. During hydrogen desorption, TiNi, which has better desorption kinetics, first dehydrides and contributes to the overall electrochemical capacity; then, the hydrogen stored in Ti_2Ni phase is transferred internally into the dehydrided portion of TiNi and discharged through TiNi. Without the assistance of TiNi phase, the hydrogen stored in Ti_2Ni phase cannot be released due to the stronger meta-hydrogen bond strength. However, the cycle stability of such a biphasic system suffers due to the corrosion and oxidation of Ti_2Ni [159,162].

Most research efforts on TiNi alloys focused on elemental modifications on both A- and B-sites. Different material manufacturing procedures, such as mechanical alloying, annealing, and different quench rates, were introduced to study the effect of structure on overall electrochemical properties. Emami *et al.* investigated the influence of Pd by partially replacing Ni [163,164]. While the unit cell of TiNi is enlarged by the larger-sized Pd, the electrochemical capacity is reduced since the Pd-substitution increases the stability of TiNi intermetallic alloy and decreases the stability of their hydrides according to the electronic calculations. Recently, a study on substituting Ni in TiNi with various modifiers revealed that Fe, Co, and Cr increase the electrochemical capacity up to 400 mAh g^{-1} with good activation performance [165]. Zhao *et al.* fabricated amorphous Ti_2Ni alloy by solid-state sintering and ball milling [166], and the resulting material shows improved cycle stability but also lower capacity compared to crystalline Ti_2Ni. Annealing treatment was then proposed in addition to sintering and ball milling, which results in a thicker oxide layer on the surface of amorphous Ti_2Ni and improves both capacity and charge retention of the alloy [167]. In order to increase the capacity, Zhao *et al.* developed another fabrication method for Ti_2Ni: induction melting, ball milling, and annealing [162]. The product is amorphous and nanocrystalline in nature and demonstrates reasonable capacity and good cycle stability; however, the highest reported capacity of 363 mAh g^{-1} for Ti_2Ni MH alloy is obtained at higher temperatures while cycle stability suffers. Zr-substitution for Ti was used as another way to potentially increase capacity and improve cycle stability of amorphous Ti_2Ni [168]. Zr was reported to destabilize amorphous Ti_2Ni phase and promote TiNi phase when partially substituting Ti in ball-milled Ti_2Ni from elemental powders [169]. An

amorphous Ti_3Ni_2 alloy was prepared to combine advantages from TiNi and Ti_2Ni, and although its capacity was lower than the crystalline form, cycle stability was much improved [170].

Ti-based icosahedral quasicrystal MH alloy, which has a crystallographically disallowed five-fold rotational symmetry, has only recently been studied for NiMH battery applications. The icosahedral phase is believed to contain much higher densities of tetrahedral interstitial sites compared to normal crystals [171]. Since hydrogen atoms enter favorably into tetrahedral sites, the icosahedral phase can absorb a large amount of hydrogen. Two recent studies, with and without milling after melt-spin, were performed varying the Zr/Ni ratio in $Ti_{45}Zr_{38}Ni_{17}$ [172,173]. All alloys consisted of 100% or close to 100% icosahedral phase and demonstrated that higher levels of Ni increase capacity up to 86 to 88 mAh g^{-1}; however, this value is dramatically lower than the theoretical capacity [172,173]. By changing the Zr/Ti ratio in $Ti_{45}Zr_{30}Ni_{25}$, it was shown that higher Zr deteriorates capacity. Also with annealing, an alloy that has been arc-melted and mechanically alloyed has higher capacity (up to 130 mAh g^{-1}) compared to an unannealed amorphous alloy [174]. Hu *et al.* improved capacity up to 278 mAh g^{-1} with decent cycle stability by adding Mn in a melt-spun TiVNi-based alloy [175]. The effect of Sc-addition was reported by the same group in TiVNi-based quasicrystal [176], with extended cycle life.

2.5. Mg-Ni-Based Alloys

Due to Mg's abundance, low cost, light weight, and high hydrogen storage capacity (2200 mAh g^{-1} theoretical electrochemical capacity [9]), Mg-based MH alloy continues to be an interesting research topic and a strong candidate for the negative electrode material of NiMH batteries. In order to be applicable for room temperature battery operation, a stoichiometry of Mg:Ni close to 1:1 is required. However, the MgNi intermetallic compound does not exist on the Mg-Ni binary phase diagram. Therefore, non-equilibrium fabrication methods, such as mechanical alloying, RF sputtering, laser ablation, and melt-spin, are often used to prepare MgNi alloys. Such material usually has a mixed structure of amorphous and nanocrystalline character. Despite the high capacity that MgNi alloy offers, its sluggish hydriding/dehydriding kinetics and poor corrosion resistance in alkaline media prevent MgNi from use in practical application. Various types of modifications to the MgNi system were studied to improve the overall electrochemical performance, such as replacements of A- (by rare earth, transition metals, or others) and B-sites (by transition metals), combinations of different fabrication procedures, and surface treatments [177]. Table 5 illustrates recent elemental substitution efforts on MgNi-based alloy. By varying the ball milling time, Anik *et al.* found that 15 h was sufficient to obtain the amorphous/nanocrystalline state [178,179]; however, 25 h was required to incorporate all Ni into the main MgNi phase. Electrochemical discharge capacity is also influenced by the milling period. The same report demonstrated that capacity increased sharply with up to 15 h milling time, stabilized with up to 25 h milling time, and decreased with further increase in milling time. Based on the role of each constituent element, a series of systematic elemental substitutions was conducted [178–181]. Anik *et al.* reported an improvement in electrochemical performance with $Mg_{0.80}Ti_{0.15}Al_{0.05}Zr_{0.05}Ni_{0.95}$ alloy (420 mAh g^{-1} and 90% capacity retaining rate at the 20th cycle) compared to the base MgNi alloy (495 mAh g^{-1} and 35% capacity retaining rate at the 20th cycle) [178,181]. The pulverization mechanism of MgNi was investigated by in-situ monitoring of hydride-dehydride cycles using acoustic

emission technique coupled with electrochemical measurement [182,183]. Unlike most cases where pulverization is caused by volume expansion and contraction with repeated hydrogenation, mechanically alloyed MgNi consists of porous agglomerates made up of many particles cold welded together, which are likely to be easily broken down by the mechanical action of hydrogen bubbles during hydrogen evolution. Hydrogen combustion synthesis was employed as another MgNi fabrication method; and with the help of subsequent ball milling and surface protection from NAFION coating, a 400% increase in capacity could be achieved [184].

Table 5. Summary of recent research on electrochemical property improvement for mechanically alloyed MgNi MH alloys.

Substitution	Alloy formula	Range of *x*	Capacity	Cycle life	Comment	Reference
Ti	$Mg_{1-x}Ti_xNi$	0 to 0.2	up then down	up	As the Ti/Mg ratio increases, surface charge transfer resistance increases	[178,180]
Ti	$Mg_{0.7}Ti_{0.3}Ni$	–	down	up	–	[185]
Ti	$Mg_{1-x}Ti_xNi$	0 to 0.1	down	up	Reduces pulverization	[186]
Zr	$Mg_{1-x}Zr_xNi$	0 to 0.2	up then down	up	–	[178]
La	$Mg_{0.7}Ti_{0.225}La_{0.075}Ni$	–	down	up	Further improves corrosion resistance	[185]
Al	$Mg_{1-x}Al_xNi$	0 to 0.2	down	up	–	[178]
Al	$Mg_{0.9}Ti_{0.1}NiAl_x$	0 to 0.05	down	up	Reduces pulverization	[187]
B	$Mg_{1-x}B_xNi$	0 to 0.2	down	same	–	[178]
Pd	$Mg_{1-x}Pd_xNi$	0 to 0.2	down	up	Surface charge transfer resistance decreases and then increases	[179]
Pd	$Mg_{0.9}Ti_{0.1}NiAl_{0.05}Pd_x$	0 to 0.1	down	up	Increases HRD	[187]
Pd	$Mg_{50}Ni_{50-x}Pd_x$	0 to 5	down	up	–	[188]
Mg/Ni	$Mg_{0.85+x}Ti_{0.15}Ni_{1.0-x}$	0 to 0.1	up	down	–	[180]

Mg_2Ni is another Mg-Ni system that has been extensively studied for its potential applications in hydrogen storage and NiMH battery. With the higher content of hydride-former in the Mg_2Ni formulation, it is capable of storing a greater amount of hydrogen compared to MgNi; however, Mg_2Ni's discharge kinetics and corrosion resistance are worse. Nanocrystalline/amorphous structure was shown to improve hydriding/dehydriding kinetics [189]; such structure can be achieved by mechanical alloying and melt-spin fabrication techniques or elemental substitution. Although the exact effect of melt-spin cooling rates depends on the type of elemental substitution, a higher cooling rate was frequently found to be beneficial in enhancing electrochemical properties and cycle stability [190–197]. Furthermore, the length of milling time plays an important role in varying the performances of mechanically alloyed materials [198,199]. Melt-spin in magnetic field has been reported to greatly improve both capacity and stability [200]. Zhu *et al.* provided a comparison among the influences of various processing methods on electrochemical characteristics [201]. Table 6 summarizes the recent elemental substitution efforts on the Mg_2Ni system. It should be noted that besides the Mg-Ni MH systems, other Mg-based alloys, such as MgTi [202] and MgAl [203] systems doped with Ni, were also investigated for their electrochemical properties.

Table 6. Summary of recent research on electrochemical property improvement for Mg_2Ni MH alloys. MS: melt-spin, MSM: melt-spin in magnetic field, HCS: hydriding combustion synthesis, BM: ball milling, MSP: magnetron sputtering.

Substitution/ Addition	Process	Alloy formula	Range of *x*	Capacity	HRD	Cycle life	Comment	Reference
Co	MS	$Mg_2Ni_{1-x}Co_x$	0 to 0.4	up	up	up	Promotes amorphous phase	[190,191,194,195]
Mn	MS	$Mg_2Ni_{1-x}Mn_x$	0 to 0.4	up	up then down	up	Promotes amorphous phase	[192,194,195]
Cu	MS	$Mg_2Ni_{1-x}Cu_x$	0 to 0.4	up	up then down	up	–	[193–195]
La	MS	$Mg_{2-x}La_xNi$	0 to 0.2	–	up	up	Promotes amorphous phase	[196,197]
–	MSM	Mg_2Ni	–	up	–	up	–	[200]
Co	HCS+BM	$Mg_{2.1-x}Co_xNi$	0 to 0.1	down	down	up	–	[204]
Cr	HCS+BM	$Mg_{2.1-x}Cr_xNi$	0 to 0.1	down	down	up	–	[204]
Nb	HCS+BM	$Mg_{2.1-x}Nb_xNi$	0 to 0.1	down	down	up	–	[204]
Ti	HCS+BM	$Mg_{2.1-x}Ti_xNi$	0 to 0.1	down	down	up	–	[204]
V	HCS+BM	$Mg_{2.1-x}V_xNi$	0 to 0.1	down	down	up	–	[204]
Al	HCS+BM	$Mg_{2-x}Al_xNi$	0 to 0.7	up then down	–	–	–	[199]
Ti	BM	$Mg_{2-x}Ti_xNi$	0 to 0.5	up	–	up	–	[198]
B	BM	$Mg_{1.5}Ti_{0.3}Zr_{0.1}Al_{0.1}Ni$	–	–	–	–	Compares to others in [205]	[205]
C	BM	$Mg_{1.5}Ti_{0.3}Zr_{0.1}Al_{0.1}Ni$	–	–	–	–	Compares to others in [205]	[205]
Fe	BM	$Mg_{1.5}Ti_{0.3}Zr_{0.1}Al_{0.1}Ni$	–	–	–	–	Compares to others in [205]	[205]
Pd	BM	$Mg_{1.5}Ti_{0.3}Zr_{0.1}Al_{0.1}Ni$	–	–	–	–	Compares to others in [205]	[205]
Al	BM	$Mg_{1.5}Ti_{0.3}Zr_{0.1}Al_{0.1}Ni$	–	–	–	–	Compares to others in [205]	[205]
Al	BM	$Mg_{2-x}Al_xNi$	0 to 0.25	up	–	–	–	[206]
Multiwalled carbon nanotubes	BM	$(MgAl)_2Ni$	–	up	–	–	–	[206]
Al	MSP	$Mg_{2-x}Al_xNi$	0 to 0.3	up then down	–	–	Improves corrosion resistance	[207]

2.6. Laves Phase-Related BCC Solid Solutions

"Laves phase-related body-centered-cubic (BCC) solid solution" [208] is an interesting MH alloy with a general formula of AB_x, where A is from Group 4A (mainly Ti), B is from Group 5A, 6A, and 7A (mainly V), and x is between 1 and 6. It has a unique two-phase microstructure composed of a BCC phase and a Laves phase (mostly C14). Microstructure evolution as a function of C14/BCC ratio is constructed based on literature review and presented in Figure 5. During solidification, the high V

BCC phase solidifies first and form a 3D framework and the rest of the liquid turns into C14 phase, which is also a complementary 3D framework, and such phenomena produces the following evolution in microstructure with the increase in C14/BCC ratio: C14 starts to appear at the grain boundary (Figure 5a) → sections of C14 phase start to connect and form a 3D network (Figure 5b) → BCC phase forms 3D framework and the cross-section is composed of isolated islands embedded in C14 matrix (Figure 5c) → BCC phase forms fish-bone type of inclusions (Figure 5d). The high density of phase boundaries contributes to the hydrogen storage properties in two ways: the promotion of a synergetic effect between BCC (high hydrogen storage capability) and C14 phases (better absorption kinetics and easy formation due to its brittleness), and the formation of a coherent and catalytic interface in between.

Figure 5. Schematics of microstructure evolution of a series of Laves phase-related body-centered-cubic (BCC) solid solution alloys as the C14 phase abundance increases (from Figure 5a–d).

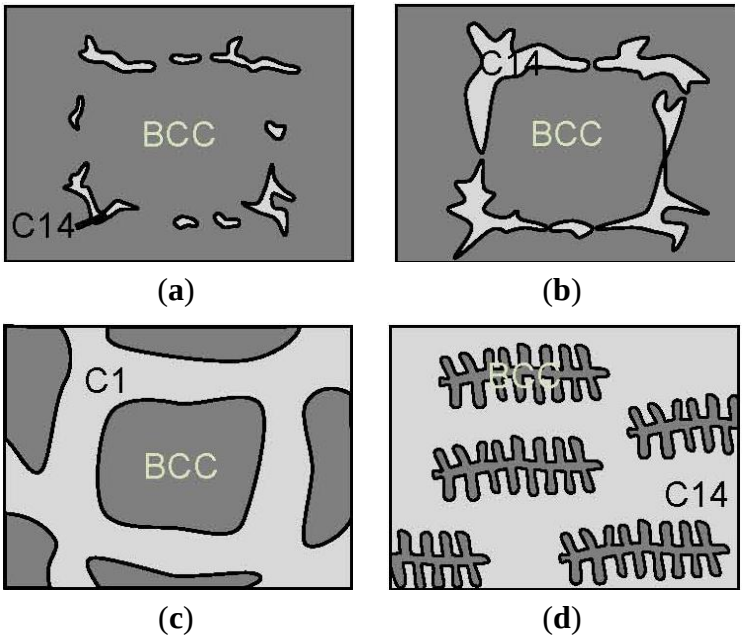

While Chai *et al.* claimed the best ratio of BCC:C14 is 1:1 for optimized results [209], Guéguen *et al.* showed that only a small amount of C14 is needed as a catalyst for the gaseous phase storage [210]. In order to study the correlation between the ratio and electrochemical properties of the alloy, we fabricated a series of Laves/BCC alloys with the Laves phase abundance from 10.5 to 91.6 wt %; their bulk diffusion coefficients and crystallite sizes are plotted in Figure 6. When one phase dominates, the crystallite size is smaller and the diffusion coefficient is larger. Therefore, a small but sufficient amount of secondary phase is preferable in the multi-phase MH alloy system. In addition, a BCC/C14 multi-phase alloy, reported by Wang and Ning, shows an electrochemical capacity of 450 mAh g^{-1}, but degradation through cycling is severe [211]. The BCC/C14 alloy was remelted with 10 wt % $LaNi_3$ [212] and up to 10 wt % $LaNi_5$ [213,214] by arc melting, and the activation behavior, HRD, low-temperature performance, and cycle life are all improved due to the synergetic effect between main and secondary phases. BCC/Ti-Ni-based multi-phase systems were also fabricated previously [117,215]. The existence of the TiNi secondary phase enhances HRD and

cycle life and shows the highest capacity of 470 mAh g^{-1} [215]. Recently, an anneal-and-quench method [216] has been implemented to prepare BCC/C14 alloys. Furthermore, quasicrystal-included alloys have also been investigated by Liu *et al.* [217–221], and capacity, HRD, and cycle stability at the 30th cycle up to 422 mAh g^{-1}, 88%, and 81%, respectively, were reported.

Figure 6. Plots of diffusion constant and crystallite size of the C14 phase determined by FWHM from XRD analysis as functions of C14 phase abundance for a series of Laves phase-related BCC solid solution alloys. The bulk transport is enhanced when the grain size is small and much of the boundary interface is available to contribute to the synergetic effect.

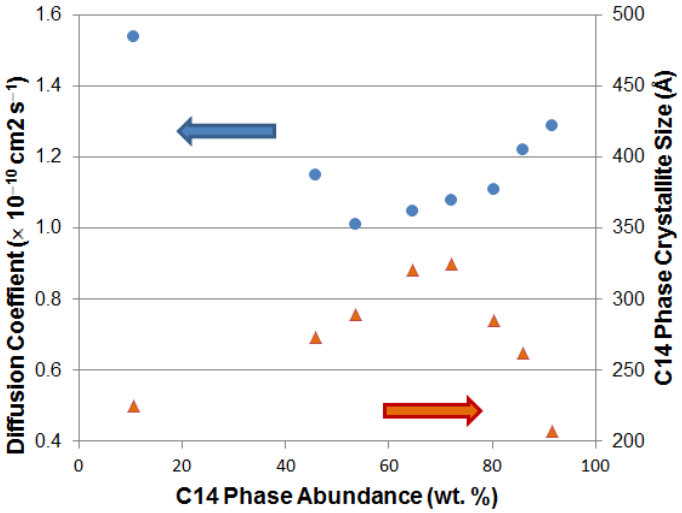

2.7. Zr-Ni-Based Alloys

Since the AB_2 intermetallic compound does not exist on the Zr-Ni binary phase diagram, one or more secondary non-Laves Zr_xNi_y phases composed of neighboring phases of AB_2 are often observed when fabricating a Zr-Ni-based MH alloy with an AB_2 composition. Between the working main phases and the catalytic secondary phases, a synergetic effect arises and contributes positively to the overall electrochemical performance. Although these minor phases do not have an appropriate metal-hydrogen bond strength when compared to the AB_2 stoichiometry, it is essential to evaluate various Zr_xNi_y alloys in order to gain better understanding of their roles in AB_2 MH alloys and potentially develop alternative rare earth-free MH alloys for NiMH battery through composition modification. A systematic examination of Zr_8Ni_{21}, Zr_7Ni_{10}, Zr_9Ni_{11}, and ZrNi alloys correlating composition, structure, gaseous phase hydrogen storage, and electrochemical properties was recently reported by Nei *et al.* [77]. Annealing is detrimental to the electrochemical capacity of Zr_xNi_y alloys due to the elimination of minor phases, similar to the annealing effect on AB_2 alloy. Furthermore, the electrochemical capacity maximizes at Zr_7Ni_{10}, which demonstrates that both hydrogen desorption/discharge rate and theoretical maximum hydrogen storage determined by the Zr/Ni ratio influence the electrochemical discharge capacity. Among all, Zr_8Ni_{21} shows the highest HRD and easiest activation. Zr_7Ni_{10} and Zr_8Ni_{21} were selected for further composition modification to improve their electrochemical properties [76,222–226], and the results are summarized in Table 7. One of the drawbacks of AB_2 alloy compared to AB_5 alloy is its lower HRD. For the purpose of increasing HRD in the Zr-based alloys, alloys with higher B/A ratios, such as $ZrNi_5$ [26] and Zr_2Ni_7 [25], become more attractive.

Performances of V-modified $ZrNi_5$ and Zr_2Ni_7 are summarized in Table 7. Although their capacities are too low for practical application (≤177 mAh g^{-1}), their bulk hydrogen diffusion properties are superior to those of existing AB_5, AB_2, and A_2B_7 alloys. With further modification, electrochemical performances of $ZrNi_5$ and Zr_2Ni_7 alloys are expected to improve.

Table 7. Summary of recent works on modification on Zr_xNi_y MH alloys.

Substitution	Alloy formula	Range of *x*	Capacity	HRD	Comment	Reference
Ti	$Ti_xZr_{7-x}Ni_{10}$	0 to 2.5	–	up	Activation becomes easier $Ti_{1.5}Zr_{5.5}Ni_{10}$ has good combination of capacity and HRD, 204 mAh g^{-1} and 79%	[76]
V	$Ti_{1.5}Zr_{5.5}V_xNi_{10-x}$	0 to 3.0	up	down	Main phase shifts from Zr_7Ni_{10} to C14 $Ti_{1.5}Zr_{5.5}V_{0.5}Ni_{9.5}$ with Zr_7Ni_{10}-predominant structure has good combination of capacity and HRD, 242 mAh g^{-1} and 80%	[222]
Cr	$Ti_{1.5}Zr_{5.5}V_{0.5}(Cr_xNi_{10-x})_{9.5}$	0.1 to 0.2	down	down	Main phase shifts from Zr_7Ni_{10} to Zr_9Ni_{11} to C14	[223,224]
Mn	$Ti_{1.5}Zr_{5.5}V_{0.5}(Mn_xNi_{10-x})_{9.5}$	0.1 to 0.2	up	up	Main phase shifts from Zr_7Ni_{10} to Zr_9Ni_{11} to C14	[223,224]
Fe	$Ti_{1.5}Zr_{5.5}V_{0.5}(Fe_xNi_{10-x})_{9.5}$	0.1 to 0.2	up	down	Main phase shifts from Zr_7Ni_{10} to C15.	[223,224]
Co	$Ti_{1.5}Zr_{5.5}V_{0.5}(Co_xNi_{10-x})_{9.5}$	0.1 to 0.2	down	down	Main phase shifts from Zr_7Ni_{10} to Zr_9Ni_{11} to C15	[223,224]
Cu	$Ti_{1.5}Zr_{5.5}V_{0.5}(Cu_xNi_{10-x})_{9.5}$	0.1 to 0.2	down	down	Main phase stays Zr_7Ni_{10}	[223,224]
Al	$Ti_{1.5}Zr_{5.5}V_{0.5}(Al_xNi_{10-x})_{9.5}$	0.1 to 0.2	down	down	Main phase shifts from Zr_7Ni_{10} to C14	[223,224]
Mg	$Zr_8Ni_{19}Mg_2$	–	down	down	Main phase shifts from Zr_8Ni_{21} to tetragonal Zr_7Ni_{10}	[225,226]
Al	$Zr_8Ni_{19}Al_2$	–	up	down	Main phase shifts from Zr_8Ni_{21} to tetragonal Zr_7Ni_{10}	[225,226]
Sc	$Zr_8Ni_{19}Sc_2$	–	down	down	Main phase shifts from Zr_8Ni_{21} to tetragonal Zr_7Ni_{10}	[225,226]
V	$Zr_8Ni_{19}V_2$	–	down	down	Main phase shifts from Zr_8Ni_{21} to Zr_2Ni_7	[225,226]
Mn	$Zr_8Ni_{19}Mn_2$	–	down	down	Main phase shifts from Zr_8Ni_{21} to Zr_2Ni_7	[225,226]
Co	$Zr_8Ni_{19}Co_2$	–	down	down	Main phase shifts from Zr_8Ni_{21} to Zr_2Ni_7	[225,226]
Sn	$Zr_8Ni_{19}Sn_2$	–	down	up	Main phase shifts from Zr_8Ni_{21} to Zr_2Ni_7 Annealed $Zr_8Ni_{19}Sn_2$ is Zr_8Ni_{21}-structured	[225,226]
La	$Zr_8Ni_{19}La_2$	–	up	down	Main phase shifts from Zr_8Ni_{21} to orthorhombic Zr_7Ni_{10}	[225,226]
Hf	$Zr_8Ni_{19}Hf_2$	–	up	down	Main phase shifts from Zr_8Ni_{21} to orthorhombic Zr_7Ni_{10}	[225,226]
V	$ZrV_xNi_{4.5-x}$	0 to 0.5	up	down	Main phase shifts from $ZrNi_5$ to monoclinic Zr_2Ni_7	[26]
V	$ZrV_xNi_{3.5-x}$	0 to 0.9	up then down	up	Main phase shifts from monoclinic Zr_2Ni_7 to cubic Zr_2Ni_7	[25]

2.8. Other Alloy Systems

It is nearly impossible to simultaneously meet all the requirements for a specific electrochemical application using one MH alloy. For example, an alloy with high capacity usually has lower HRD, and good activation behavior usually indicates shorter cycle life. Therefore, the development of composite MH alloys, which contain two or more hydrogen storage materials/intermetallic compounds/elements, can potentially combine the advantages of constituted alloys. Recent composite alloy studies include BCC related alloys modified by AB_2 (Section 2.6), AB_5 [227], $LaNi_5$ [213,214], ZrV_2 [220], A_2B_7-type [217], $LaNi_3$ [212], or other BCC [218], A_2B_7-type alloy modified by AB_5 [228], MgNi alloy modified by Ti(NiCo) [229], Mg_2Ni alloys modified by TiNi, TiFe [230], $(MgMn)_2Ni$ [231], $(MgAl)_2Ni$ [232], Co, or Ti [233], and are summarized in Table 8.

Researchers have ventured out of well-understood MH alloy systems in order to develop a novel material that fulfills all requirements of electrochemical applications. R_6T_{23} systems (R = Gd, Ho, T = Mn, Fe) were recently studied. He *et al.* performed B-site substitution using Co on Ho_6Fe_{23} and found that the alloys have Th_6Mn_{23}-type structure [234]. As the level of Co increases, activation, capacity (443 mAh g^{-1} at 150 mA g^{-1}), cycle stability, and HRD all improve. Electrochemical results were also reported on the Gd-Co-Mn system, and a promising capacity of 377 mAh g^{-1} at 150 mA g^{-1} was obtained [235]. The HRD of this type of alloy, however, is relatively low and in the range of 50% to 60%.

Table 8. Summary of recent research on composite alloys. BM: ball milling, AM: arc melting, ERM: electric resistance melting, IEC: isothermal evaporation casting.

Addition	Process	Base alloy	Addition level	Phase distribution	Capacity	HRD	Cycle life	Reference
$MmNi_{3.99}Al_{0.29}Mn_{0.3}Co_{0.6}$	BM	$Ti_{0.32}Cr_{0.43-x-y}V_{0.25}Fe_xMn_y$	0 to 20 wt %	BCC	up	–	–	[227]
$LaNi_5$	AM	$Ti_{0.10}Zr_{0.15}V_{0.35}Cr_{0.10}Ni_{0.30}$	0 to 10 wt %	BCC+C14+Zr-rich	up then down	up	up	[213,214]
ZrV_2	BM	$Ti_{1.4}V_{0.6}Ni$	0 to 20 wt %	quasicrystal+Ti_2Ni+BCC+C14+C15	up	up	up	[220]
$La_{0.65}Nd_{0.12}Mg_{0.23}Ni_{2.9}Al_{0.1}$	BM	$Ti_{1.4}V_{0.6}Ni$	0 to 20 wt %	quasicrystal+Ti_2Ni+BCC+$LaNi_5$+$PuNi_3$	same	up	down	[217]
$LaNi_3$	AM	$Ti_{0.10}Zr_{0.15}V_{0.35}Cr_{0.10}Ni_{0.30}$	0 to10 wt %	BCC+C14+Zr-rich	up	up	up	[212]
$Ti_{15}Zr_{18}V_{18}Ni_{29}Cr_5Co_7Mn$	BM	$Ti_{1.4}V_{0.6}Ni$	0 to 40 wt %	quasicrystal+Ti_2Ni+BCC+C14	up	up	up	[218]
$La_{0.377}Ce_{0.389}Pr_{0.063}Pr_{0.171}Ni_{3.5}Co_{0.6}Mn_{0.4}Al_{0.5}$	BM	$Mm_{0.80}Mg_{0.20}Ni_{2.56}Co_{0.50}Mn_{0.14}Al_{0.12}$	0 to 30 wt %	$LaNi_5$+La_2Ni_7	down	up then down	up	[228]
$TiNi_{0.56}Co_{0.44}$	BM	MgNi	0 to 50 wt %	Amorphous MgNi	down		up	[229]
TiNi	BM	Mg_2Ni	0 to 100 mol %	TiNi+Mg_2Ni	down			[230]
TiFe	BM	Mg_2Ni	0 to 100 mol %	TiFe+Mg_2Ni	up			[230]
Mg_3MnNi_2	ERM+IEC	Mg_2Ni	0 to 100 mol %	Mg_2Ni → Mg_2Ni+Mg_3MnNi_2 → Mg_3MnNi_2	up		up	[231]
Mg_3AlNi_2	ERM+IEC	Mg_2Ni	0 to 100 mol %	Mg_2Ni → Mg_2Ni+Mg_3AlNi_2 → Mg_3AlNi_2	up		up then down	[232]
Co	BM	Mg_3MnNi_2	0 to 200 mol %	amorphous Mg_3MnNi_2	up		up	[233]
Ti	BM	Mg_3MnNi_2	0 to 200 mol %	amorphous Mg_3MnNi_2	up		up	[233]

3. Conclusions

Hydrogen storage alloys for electrochemical application have been extensively studied for many years. We have presented a review of recent research activities on metal hydride alloys for nickel metal hydride battery and also provided an overview of the use of metal hydrides in other electrochemical applications. AB_5 and AB_2 alloys are very well established systems. In order to potentially dominate the future electric vehicle and stationary applications, self-discharge, low-temperature performance, and cycle stability become more important to study, and the trend of recent research reflects the efforts on improving the aforementioned properties. Superlattice A_2B_7-type alloy, which possesses the advantages of both AB_5 and AB_2 and low self-discharge capability, is likely to be the next generation of metal hydride alloy used as the negative electrode material in nickel metal hydride batteries and has attracted much attention. Although the Ti-Ni alloy system is difficult to process and has poorer high-rate performance, its much lower raw material cost makes the system one that merits further studies for improvement. The Mg-Ni alloy system holds great promise in achieving very high capacity, and recent research efforts have concentrated on improving its kinetics and cycle capability for the purpose of practical implementation. Laves phase-related BCC solid solution has high capacity; enhancing its stability is currently the most essential topic. The incorporation of quasicrystals by various fabrication methods remains an interesting subject. Zr-Ni alloy systems were systematically investigated in the last few years. Although their performance might not be satisfactory for electrochemical applications at the present time, further elemental modifications or use as a composite modifier can assist in realizing their potential.

Acknowledgments

The authors are obliged to the current and former colleagues at Ovonic for sharing the joy and hard work of NiMH battery research. They are: Stanford R. Ovshinsky, Michael A. Fetcenko, Benjamin Reichman, Cristian Fierro, Baoquan Huang, Taihei Ouchi, Su Cronogue, Jun Im, Cheng Tung, Feng Li, William Mays, John Koch, Diana Wong, and Melanie Rainhout. We also appreciate the fruitful discussions with experts outside Ovonic, which include: Koiji Morii from Daido Steel, Hongge Pan from Zhejiang University, Shigekazu Yasuoka and Kazuta Takeno from FDK-Twicell, Lingkun Kong from Shenzhen High Power, Aishen Wu from Shida Battery, Xilin Zhu from REO MH Alloy Co., David Zheng from Gold Peak, Leonid Bendersky from NIST, Simon Ng, Steve Sally, and Gavin Lawes from Wayne State University, and Yi Liu from Oregon State University.

Conflicts of Interest

The authors declare no conflict of interest.

References

1. Schmitt, R. Process for manufacturing a negative accumulator electrode for the reversible storage and restitution of hydrogen. U.S. Patent 3,972,726A, 3 August 1976.
2. Willems, J.G. Metal hydride electrodes stability of $LaNi_5$-related compounds. *Philips J. Res.* **1984**, *39*, 1–94.

3. Anani, A.; Visintin, A.; Petrov, K.; Srinivasan, S.; Reilly, J.J.; Johnson, J.R.; Schwarz, R.B.; Desch, P.B. Alloys for hydrogen storage in nickel/hydrogen and nickel/metal hydride batteries. *J. Power Sources* **1994**, *47*, 261–275.
4. Kleperis, J.; Wójcik, G.; Czerwinski, A.; Skowronski, J.; Kopczyk, M.; Beltowska-Brzezinska, M. Electrochemical behavior of metal hydride. *J. Solid State Electrochem.* **2001**, *5*, 229–249.
5. Feng, F.; Geng, M.; Northwood, D.O. Electrochemical behaviour of intermetallic-based metal hydrides used in Ni/metal hydride (MH) batteries: A review. *Int. J. Hydrog. Energy* **2001**, *26*, 725–734.
6. Hong, K. The development of hydrogen storage electrode alloys for nickel hydride batteries. *J. Power Sources* **2001**, *96*, 85–89.
7. Cuevas, F.; Joubert, J.M.; Latroche, M.; Percheron-Guégan, A. Intermetallic compounds as negative electrodes of Ni/MH batteries. *Appl. Phys. A* **2001**, *72*, 225–238.
8. Petrii, O.A.; Levin, E.E. Hydrogen-accumulating materials in electrochemical systems. *Russ. J. General Chem.* **2007**, *77*, 790–796.
9. Zhao, X.; Ma, L. Recent progress in hydrogen storage alloys for nickel/metal hydride secondary batteries. *Int. J. Hydrog. Energy* **2009**, *34*, 4788–4796.
10. Liu, Y.; Pan, H.; Gao, M.; Wang, Q. Advanced hydrogen storage alloys for Ni/MH rechargeable batteries. *J. Mater. Chem.* **2011**, *21*, 4743–4755.
11. Wessells, C.; Ruffo, R.; Huggins, R.A.; Cui, Y. Investigations of the electrochemical stability of aqueous electrolytes for lithium battery applications. *Electrochem. Solid-State Lett.* **2010**, *13*, A59–A61.
12. Nakayama, H.; Nobuhara, K.; Kon, M.; Matsunaga, T. *Electrochemical Properties of Metal Hydrides as Anode for Rechargeable Lithium Ion Batteries*; The Electrochemical Society: Susono, Shizuoka, Japan, 2010; p. 1052.
13. Dong, H.; Kiros, Y.; Noréus, D. An air-metal hydride battery using $MmNi_{3.6}Mn_{0.4}Al_{0.3}Co_{0.7}$ in the anode and a perovskite in the cathode. *Int. J. Hydrog. Energy* **2010**, *35*, 4336–4341.
14. Mizutani, M.; Morimitsu, M. *Development of a Metal Hydride/Air Secondary Battery with Multiple Electrodes*; The Electrochemical Society: Las Vegas, NV, USA, 2010; p. 453.
15. Osada, N.; Morimitsu, M. *Cycling Performance of Metal Hydride-Air Rechargeable Battery*; The Electrochemical Society: Las Vegas, NV, USA, 2010; p. 194.
16. Weng, G.; Li, C.V.; Chan, K. *High Efficiency Vanadium-Metal Hydride hybrid Flow Battery: Importance in Ion Transport and Membrane Selectivity*; The Electrochemical Society: Toronto, ON, Canada, 2013; p. 242.
17. Weng, G.; Li, C.V.; Chan, K. *Study of the Electrochemical Behavior of high Voltage Vanadium-Metal hydride Hybrid Flow Battery*; The Electrochemical Society: Toronto, ON, Canada, 2013; p. 484.
18. Weng, G.; Li, C.V.; Chan, K. *Exploring the Role of Ionic Interfaces of the High Voltage Lead Acid-Metal Hydride Hybrid Battery*; The Electrochemical Society: Hilton Hawaiian Village, HI, USA, 2012; p. 372.
19. Purushothama, B.K.; Wainright, J.S. Analysis of pressure variations in a low-pressure nickel-hydrogen battery. Part 2: Cells with metal hydride storage. *J. Power Sources* **2012**, *206*, 421–428.

20. Danko, D.B.; Sylenko, P.M.; Shlapak, A.M.; Khyzhun, O.Y.; Shcherbakova, L.G.; Ershova, O.G.; Solonin, Y.M. Photoelectrochemical cell for water decomposition with a hybrid photoanode and a metal-hydride cathode. *Solar Energy Mater. Solar Cells* **2013**, *114*, 172–178.
21. Beccu, K. Accumulator electrode with capacity for storing hydrogen and method of manufacturing said electrode. U.S. Patent 3,669,745A, 3 June 1972.
22. Willems, J.J.G.; Buschow, K.H.J. From permanent magnets to rechargeable hydride electrodes. *J. Less Common Metals* **1987**, *129*, 13–30.
23. Young, K.; Huang, B.; Regmi, R.K.; Lawes, G.; Liu, Y. Comparisons of metallic clusters imbedded in the surface of AB_2, AB_5, and A_2B_7 alloys. *J. Alloy. Compd.* **2010**, *506*, 831–840.
24. Young, K.; Ouchi, T.; Huang, B. Effects of annealing and stoichiometry to (Nd, Mg)(Ni, Al)$_{3.5}$ metal hydride alloys. *J. Power Sources* **2012**, *215*, 152–159.
25. Young, M.; Chang, S.; Young, K.; Nei, J. Hydrogen storage properties of $ZrV_xNi_{3.5-x}$ (x = 0.0–0.9) metal hydride alloys. *J. Alloy. Compd.* **2013**, in press.
26. Young, K.; Young, M.; Chang, S.; Huang, B. Synergetic effects in electrochemical properties of $ZrV_xNi_{4.5-x}$ (x = 0.0, 0.1, 0.2, 0.3, 0.4, and 0.5) metal hydride alloys. *J. Alloy. Compd.* **2013**, *560*, 33–41.
27. Van Vucht, J.H.N.; Kuijpers, F.A.; Burning, H.C.A.M. Reversible room-temperature absorption of large quantities of hydrogen by intermetallic compounds. *Philips Res. Rep.* **1970**, *25*, 133–140.
28. Young, K.; Ouchi, T.; Reichman, B.; Koch, J.; Fetcenko, M.A. Improvement in the low-temperature performance of AB_5 metal hydride alloys by Fe-addition. *J. Alloy. Compd.* **2011**, *509*, 7611–7617.
29. Young, K.; Ouchi, T.; Banik, A.; Koch, J.; Fetcenko, M.A.; Bendersky, L.A.; Wang, K.; Vaudin, M. Gas atomization of Cu-modified AB_5 metal hydride alloys. *J. Alloy. Compd.* **2011**, *509*, 4896–4904.
30. Young, K.; Ouchi, T.; Reichman, B.; Koch, J.; Fetcenko, M.A. Effects of Mo additive on the structure and electrochemical properties of low-temperature AB_5 metal hydride alloys. *J. Alloy. Compd.* **2011**, *509*, 3995–4001.
31. Kong, L.; Chen, B.; Young, K.; Koch, J.; Chan, A.; Li, W. Effects of Al- and Mn-contents in the negative MH alloy on the self-discharge and long-term storage properties of Ni/MH battery. *J. Power Sources* **2012**, *213*, 128–139.
32. Young, K.; Huang, B.; Ouchi, T. Studies of Co, Al, and Mn substitutions in $NdNi_5$ metal hydride alloys. *J. Alloy. Compd.* **2012**, *543*, 90–98.
33. Liu, B.; Li, A.; Fan, Y.; Hu, M.; Zhang, B. Phase structure and electrochemical properties of $La_{0.7}Ce_{0.3}Ni_{3.75}Mn_{0.35}Al_{0.15}Cu_{0.75-x}Fe_x$ hydrogen storage alloys. *Trans. Nonferrous Metals Soc. China* **2012**, *22*, 2730–2735.
34. Peng, X.; Liu, B.; Fan, Y.; Ji, L.; Zhang, B.; Zhang, Z. Phase structure and electrochemical hydrogen storage characteristics of $La_{0.7}Ce_{0.3}Ni_{3.85}Mn_{0.8}Cu_{0.4}Fe_{0.15-x}(Fe_{0.43}B_{0.57})_x$ (x = 0–0.15) alloys. *Int. J. Electrochem. Sci.* **2013**, *8*, 3419–3428.
35. Fan, Y.; Liu, B.; Zhang, B.; Ji, L.; Wang, Y.; Zhang, Z. Microstructures and electrochemical properties of $LaNi_{3.55}Co_{0.2-x}Mn_{0.35}Al_{0.15}Cu_{0.75}(Fe_{0.43}B_{0.57})_x$ (x = 0–0.20) hydrogen storage alloys. *Mater. Chem. Phys.* **2013**, *138*, 803–809.

36. Liu, B.; Peng, X.; Fan, Y.; Ji, L.; Zhang, B.; Zhang, Z. Microstructures and electrochemical properties of $LaNi_{3.55}Co_{0.2-x}Mn_{0.35}Al_{0.15}Cu_{0.75}(V_{0.81}Fe_{0.19})_x$ hydrogen storage alloys. *Int. J. Electrochem. Sci.* **2012**, *7*, 11966–11977.
37. Liu, B.; Hu, M.; Fan, Y.; Ji, L.; Zhu, X.; Li, A. Microstructures and electrochemical properties of $La_{0.7}Ce_{0.3}Ni_{3.75-x}Cu_{0.75}Mn_{0.35}Al_{0.15}(Fe_{0.43}B_{0.57})_x$ hydrogen storage alloys. *Electrochim. Acta* **2012**, *69*, 384–388.
38. Wang, Y.; Fan, Y.; Li, A. Phase structure and electrochemical properties of $La_{0.7}Ce_{0.3}Ni_{3.83-x}Mn_{0.43}Co_{0.25}Al_{0.26}Cu_{0.48}(Fe_{0.43}B_{0.57})_x$ hydrogen storage alloys. *Int. J. Electrochem. Sci*. **2013**, *8*, 5469–5478.
39. Liu, B.; Hu, M.; Zhou, Y.; Li, A.; Ji, L.; Fan, Y.; Zhang, Z. Microstructures and electrochemical characteristics of $La_{0.7}Ce_{0.3}Ni_{3.75-x}Cu_{0.75}Mn_{0.35}Al_{0.15}(V_{0.81}Fe_{0.19})_x$ (x = 0–0.20) hydrogen storage alloys. *J. Alloy. Compd.* **2012**, *544*, 105–110.
40. Peng, X.; Liu, B.; Fan, Y.; Ji, L.; Zhang, B.; Zhang, Z. Microstructures and electrochemical characteristics of $La_{0.7}Ce_{0.3}Ni_{4.2}Mn_{0.9-x}Cu_{0.37}(V_{0.81}Fe_{0.19})_x$ hydrogen storage alloys. *Electrochim.Acta* **2013**, *93*, 207–212.
41. Peng, X.; Liu, B.; Fan, Y.; Zhu, X.; Peng, Q.; Zhang, Z. Microstructures and electrochemical hydrogen storage characteristics of $La_{0.7}Ce_{0.3}Ni_{4.2}Mn_{0.9-x}Cu_{0.37}(Fe_{0.43}B_{0.57})_x$ (x = 0–0.20) alloys. *J. Power Sources* **2013**, *240*, 178–183.
42. Liu, B.; Hu, M.; Ji, L.; Fan, Y.; Wang, Y.; Zhang, Z.; Li, A. Phase structure and electrochemical properties of $La_{0.7}Ce_{0.3}Ni_{3.75}Mn_{0.35}Al_{0.15}Cu_{0.75-x}(Fe_{0.43}B_{0.57})_x$ hydrogen storage alloys. *J. Alloy. Compd.* **2012**, *516*, 53–57.
43. Liu, B.; Hu, M.; Li, A.; Ji, L.; Zhang, B.; Zhu, X. Microstructure and electrochemical characteristics of $La_{0.7}Ce_{0.3}Ni_{3.75}Mn_{0.35}Al_{0.15}Cu_{0.75-x}(V_{0.81}Fe_{0.19})_x$ hydrogen storage alloys. *J. Rare Earths* **2012**, *30*, 769–774.
44. Fan, Y.; Liu, B.; Zhang, B.; Ji, L.; Zhang, Z. Phase structure and electrochemical properties of non-stoichiometric $La_{0.7}Ce_{0.3}(Ni_{3.65}Cu_{0.75}Mn_{0.35}Al_{0.15}(Fe_{0.43}B_{0.57})_{0.10})_x$ hydrogen storage alloys. *J. Rare Earths* **2012**, *30*, 1249–1254.
45. Zhang, B.; Wu, W.; Bian, X.; Tu, G. Investigations on the kinetics properties of the electrochemical reactions of $MlNi_{3.55}Co_{0.75-x}Mn_{0.4}Al_{0.3}(Cu_{0.75}P_{0.25})_x$ (x = 0.0, 0.1, 0.2, 0.3, 0.4) hydrogen storage alloys. *J. Alloy. Compds* **2012**, *538*, 189–192.
46. Zhang, B.; Wu, W.; Bian, X.; Tu, G. Study on microstructure and electrochemical performance of the $MlNi_{3.55}Co_{0.75-x}Mn_{0.4}Al_{0.3}(Cu_{0.75}P_{0.25})_x$ (x = 0–0.5) composite alloys. *J. Power Sources* **2013**, *236*, 80–86.
47. Drulis, H.; Hackemer, A.; Folcik, L.; Giza, K.; Bala, H.; Gondek, Ł.; Figiel, H. Thermodynamic and electrochemical hydrogenation properties of $LaNi_{5-x}In_x$ alloys. *Int. J. Hydrog. Energy* **2012**, *37*, 15850–15854.
48. Giza, K.; Bala, H.; Drulis, H.; Hackemer, A.; Folcik, L. Gaseous and electrochemical hydrogenation properties of $LaNi_{4.3}(Co, Al)_{0.7-x}In_x$ alloys. *Int. J. Electrochem. Sci.* **2012**, *7*, 9881–9891.
49. Balogun, M.; Wang, Z.; Huang, H.; Liu, W.; Ni, C.; Li, G. Microstructure and electrode performance of $LaNi_{4.1-x}Co_{0.6}Mn_{0.3}Al_x$ hydrogen storage alloys. *J. Guilin Univ. Electron. Technol.* **2012**, *32*, 508–513.

50. Chao, D.; Zhong, C.; Ma, Z.; Yang, F.; Wu, Y.; Zhu, D.; Wu, C.; Chen, Y. Improvement in high-temperature performance of Co-free high-Fe AB_5-type hydrogen storage alloys. *Int. J. Hydrog. Energy* **2012**, *37*, 12375–12383.
51. Balogun M.; Wang, Z.; Chen, H.; Deng, J.; Yao, Q.; Zhou, H. Effect of Al content on structure and electrochemical properties of $LaNi_{4.4-x}Co_{0.3}Mn_{0.3}Al_x$ hydrogen storage alloys. *Int. J. Hydrog. Energy* **2013**, *39*, 10926–10931.
52. Yang, S.; Han, S.; Li, Y.; Yang, S.; Hu, L. Effect of substituting B for Ni on electrochemical kinetic properties of AB_5-type hydrogen storage alloys for high-power nickel/metal hydride batteries. *Mater. Sci. Eng. B* **2011**, *176*, 231–236.
53. Yang, S.; Han, S.; Song, J.; Li, Y. Influences of molybdenum substitution for cobalt on the phrase structure and electrochemical kinetic properties of AB_5-type hydrogen storage alloys. *J. Rare Earths* **2011**, *29*, 692–697.
54. Srivastava, S.; Upadhyay, R.K. Investigations of AB_5-type negative electrode for nickel-metal hydride cell with regard to electrochemical and microstructural characteristics. *J. Power Sources* **2010**, *195*, 2996–3001.
55. Peng, X.; Liu, B.; Zhou, Y.; Fan, Y.; Yang, Y.; Li, Q. Microstructures and electrochemical hydrogen storage characteristics of $La_{0.65-x}Ce_{0.25-x}Pr_{0.03}Nd_{0.07}Y_{2x}Ni_{3.65}Co_{0.75}Mn_{0.3}Al_{0.3}$ (x = 0–0.04) alloys. *Int. J. Electrochem. Sci.* **2013**, *8*, 2262–2271.
56. Du, Y.; Li, W. Structural and electrochemical properties of annealed $La_{1-x}Y_xNi_{3.55}Mn_{0.4}Al_{0.3}Co_{0.75}$ hydrogen storage alloys. *J. Environ. Sci.* **2011**, *23*, S59–S62.
57. Takasaki, T.; Nishimura, K.; Saito, M.; Fukunaga, H.; Iwaki, T.; Sakai, T. Cobalt-free nickel-metal hydride battery for industrial applications. *J. Alloy. Compd.* **2013**. Available online: http://dx.doi.org/10.1016/j.jallcom.2013.01.092 (accessed on 4 July 2013).
58. Su, G.; He, Y.; Liu, K. Effects of pretreatment on $MlNi_{4.00}Co_{0.45}Mn_{0.38}Al_{0.3}$ hydrogen storage alloy powders and the performance of 6 Ah prismatic traction battery. *Int. J. Hydrog. Energy* **2012**, *37*, 12384–12392.
59. Tian, X.; Liu, X.; Yao, Z.; Yan, S. Structure and electrochemical properties of rapidly quenched $Mm_{0.3}Ml_{0.7}Ni_{3.55}Co_{0.75}Mn_{0.4}Al_{0.3}$ hydrogen storage alloy. *J. Mater. Eng. Perform.* **2013**, *22*, 848–853.
60. Yang, S.; Liu, Z.; Han, S.; Zhang, W.; Song, J. Effects of annealing treatment on the microstructure and electrochemical properties of low-Co hydrogen storage alloys containing Cu and Fe. *Rare Metals* **2011**, *30*, 464–469.
61. Kim, J.; Yamamoto, K.; Yonezawa, S.; Takashima, M. Effects of Ni-PTFE composite plating on AB_5-type hydrogen storage alloy. *Mater. Lett.* **2012**, *82*, 217–219.
62. Cuscueta, D.J.; Corso, H.L.; Arenillas, A.; Martinez, P.S.; Ghilarducci, A.A.; Salva, H.R. Electrochemical effect of carbon nanospheres on an AB_5 alloy. *Int. J. Hydrog. Energy* **2012**, *37*, 14978–14982.
63. Li, X.; Wang, L.; Dong, H.; Song, Y.; Shang, H. Electrochemical hydrogen absorbing properties of graphite/AB_5 alloy composite electrode. *J. Alloy. Compd.* **2012**, *510*, 114–118.
64. Jang, I.; Kalubarme, R.S.; Yang, D.; Kim, T.; Park, C.; Ryu, H.; Park, C. Mechanism for the degradation of $MmNi_{3.9}Co_{0.6}Mn_{0.3}Al_{0.2}$ electrode and effects of additives on electrode degradation for Ni-MH secondary batteries. *Metals Mater. Int.* **2011**, *17*, 891–897.

65. Zhang, Q.; Su, G.; Li, A.; Liu, K. Electrochemical performances of AB_5-type hydrogen storage alloy modified with Co_3O_4. *Trans. Nonferrous Metals Soc. China* **2011**, *21*, 1428–1434.
66. Su, G.; He, Y.; Liu, K. Effects of Co_3O_4 as additive on the performance of metal hydride electrode and Ni-MH battery. *Int. J. Hydrog. Energy* **2012**, *37*, 11994–12002.
67. Yun, L.; Xing, K.; Feng, H. Impact of hydroxy Ni powders on electrochemical properties of AB_5 hydrogen storage alloy. *Value Eng.* **2013**, *30*, 288–289.
68. Nei, J.; Young, K.; Salley, S.O.; Ng, K.Y.S. Determination of C14/C15 phase abundance in Laves phase alloys. *Mater. Chem. Phys.* **2012**, *136*, 520–527.
69. Boettinger, W.J.; Newbury, D.E.; Wang, K.; Bendersky, L.A.; Chiu, C.; Kanttner, U.R.; Young, K.; Chao, B. Examination of multiphase $(Zr,Ti)(V,Cr,Mn,Ni)_2$ Ni-MH electrode alloys: Part I. Dendritic solidification structure. *Metall. Mater. Trans. A* **2010**, *41*, 2033–2047.
70. Bendersky, L.A.; Wang, K.; Boettinger, W.J.; Newbury, D.E.; Young, K.; Chao, B. Examination of multiphase $(Zr,Ti)(V,Cr,Mn,Ni)_2$ Ni-MH electrode alloys: Part II. Solid-state transformation of the interdendritic B2 phase. *Metall. Mater. Trans. A* **2010**, *41*, 1891–1906.
71. Bendersky, L.A.; Wang, K.; Boettinger, W.J; Bewbury, D.E.; Young, K.; Chao, B. Microstructural Studies of Multiphase $(Zr,Ti)(V,Cr,Mn,Co,Ni)_2$ Alloys for Ni/MH Negative Electrodes. In *Intermetallic-Based Alloys for Structural and Functional Applications*; Bewlay, P., Kumar, Y., Eds.; MRS: Boston, MA, USA, 2010; Volume 1295.
72. Bendersky, L.A.; Wang, K.; Levin, I.; Newbury, D.; Young, K.; Chao, B.; Creuziger, A. $Ti_{12.5}Zr_{21}V_{10}Cr_{8.5}Mn_xCo_{1.5}Ni_{46.5-x}$ AB_2-type metal hydride alloys for electrochemical storage application: Part 1. Structural characteristics. *J. Power Sources* **2012**, *218*, 474–486.
73. Young, K.; Ouchi, T.; Huang, B.; Chao, B.; Fetcenko, M.A.; Bendersky, L.A.; Wang, K.; Chiu, C. The correlation of C14/C15 phase abundance and electrochemical properties in the AB_2 alloys. *J. Alloy. Compd.* **2010**, *506*, 841–848.
74. Young, K.; Nei, J.; Ouchi, T.; Fetcenko, M.A. Phase abundances in AB_2 metal hydride alloys and their correlations to various properties. *J. Alloy. Compd.***2011**, *509*, 2277–2284.
75. Young, K.; Chao, B.; Bendersky, L.A.; Wang, K. $Ti_{12.5}Zr_{21}V_{10}Cr_{8.5}Mn_xCo_{1.5}Ni_{46.5-x}$ AB_2-type metal hydride alloys for electrochemical storage application: Part 2. Hydrogen storage and electrochemical properties. *J. Power Sources* **2012**, *218*, 487–494.
76. Young, K.; Ouchi, T.; Liu, Y.; Reichman, B.; Mays, W.; Fetcenko, M.A. Structural and electrochemical properties of $Ti_xZr_{7-x}Ni_{10}$. *J. Alloy. Compd.* **2009**, *480*, 521–528.
77. Nei, J.; Young, K.; Regmi, R.; Lawes, G.; Salley, S.O.; Ng, K.Y.S. Gaseous phase hydrogen storage and electrochemical properties of Zr_8Ni_{21}, Zr_7Ni_{10}, Zr_9Ni_{11}, and ZrNi metal hydride alloys. *Int. J. Hydrog. Energy* **2012**, *37*, 16042–16055.
78. Young, K.; Ouchi, T.; Yang, J.; Fetcenko, M.A. Studies of off-stoichiometric AB_2 metal hydride alloy: Part 1. Structural characteristics. *Int. J. Hyrdog. Energy* **2011**, *36*, 11137–11145.
79. Young, K.; Nei, J.; Huang, B.; Fetcenko, M.A. Studies of off-stoichiometric AB_2 metal hydride alloy: Part 2. Hydrogen storage and electrochemical properties. *Int. J. Hydrog. Energy* **2011**, *36*, 11146–11154.
80. Young, K.; Ouchi, T.; Fetcenko, M.A. Pressure-composition-temperature hysteresis in C14 Laves phase alloys: Part 1. Simple ternary alloys. *J. Alloy. Compd.* **2009**, *480*, 428–433.

81. Young, K.; Ouchi, T.; Mays, W.; Reichman, B.; Fetcenko, M.A. Pressure-composition-temperature hysteresis in C14 Laves phase alloys: Part 2. Applications in NiMH batteries. *J. Alloy. Compd.* **2009**, *480*, 434–439.
82. Young, K.; Ouchi, T.; Fetcenko, M.A. Pressure-composition-temperature hysteresis in C14 Laves phase alloys: Part 3. Empirical formula. *J. Alloy. Compd.* **2009**, *480*, 440–448.
83. Young, K.; Koch, J.; Ouchi, T.; Banik, A.; Fetcenko, M.A. Study of AB_2 alloy electrodes for Ni/MH battery prepared by centrifugal casting and gas atomization. *J. Alloy. Compd.* **2010**, *496*, 669–677.
84. Young, K.; Ouchi, T.; Banik, A.; Koch, J.; Fetcenko, M.A. Improvement in the electrochemical properties of gas atomized AB_2 metal hydride alloys by hydrogen annealing. *Int. J. Hydrog. Energy* **2011**, *36*, 3547–3555.
85. Young, K.; Ouchi, T.; Huang, B.; Fetcenko, M.A. Effects of B, Fe, Gd, Mg, and C on the structure, hydrogen storage, and electrochemical properties of vanadium-free AB_2 metal hydride alloy. *J. Alloy. Compd.* **2012**, *511*, 242–250.
86. Young, K.; Ouchi, T.; Koch, J.; Fetcenko, M.A. Compositional optimization of vanadium-free hypo-stoichiometric AB_2 metal hydride alloy for Ni/MH battery application. *J. Alloy. Compd.* **2012**, *510*, 97–106.
87. Young, K.; Fetcenko, M.A.; Koch, J.; Morii, K.; Shimizu, T. Studies of Sn, Co, Al, and Fe additives in C14/C15 Laves alloys for NiMH battery application by orthogonal arrays. *J. Alloy. Compd.* **2009**, *486*, 559–569.
88. Young, K.; Regmi, R.; Lawes, G.; Ouchi, T.; Reichman, B.; Fetcenko, M.A.; Wu, A. Effects of aluminum substitution in C14-rich multi-component alloys for NiMH battery application. *J. Alloy. Compd.* **2010**, *490*, 282–292.
89. Young, K.; Ouchi, T.; Fetcenko, M.A. Roles of Ni, Cr, Mn, Sn, Co, and Al in C14 Laves phase alloys for NiMH battery application. *J. Alloy. Compd.* **2009**, *476*, 774–781.
90. Young, K.; Ouchi, T.; Reichman, B.; Mays, W.; Regmi, R.; Lawes, G.; Fetcenko, M.A.; Wu, A. Optimization of Co-content in C14 Laves phase multi-component alloys for NiMH battery application. *J. Alloy. Compd.* **2010**, *489*, 202–210.
91. Young, K.; Ouchi, T.; Huang, B.; Reichman, B.; Fetcenko, M.A. Effect of molybdenum content on structural, gaseous storage, and electrochemical properties of C14-predominant AB_2 metal hydride alloys. *J. Power Sources* **2011**, *196*, 8815–8821.
92. Young, K.; Ouchi, T.; Huang, B.; Reichman, B.; Fetcenko, M.A. Studies of copper as a modifier in C14-predominant AB_2 metal hydride alloys. *J. Power Sources* **2012**, *204*, 205–212.
93. Young, K.; Ouchi, T.; Huang, B.; Reichman, B.; Fetcenko, M.A. The structure, hydrogen storage, and electrochemical properties of Fe-doped C14-predominating AB_2 metal hydride alloys. *Int. J. Hydrog. Energy* **2011**, *36*, 12296–12304.
94. Young, K.; Wong, D.F.; Ouchi, T.; Huang, B.; Reichman, B.; Fetcenko, M.A. Effects of La-addition to the structure, hydrogen storage, and electrochemical properties of C14 metal hydride alloys. *J. Alloy. Compd.* Submitted.
95. Young, K.; Ouchi, T.; Koch, J.; Fetcenko, M.A. The role of Mn in C14 Laves phase multi-component alloys for NiMH battery application. *J. Alloy. Compd.* **2009**, *477*, 749–758.

96. Ruiz, F.C.; Peretti, H.A.; Visintin, A.; Triaca, W.E. A study on $ZrCrNiPt_x$ alloys as negative electrode components for NiMH batteries. *Int. J. Hydrog. Energy* **2011**, *36*, 901–906.
97. Young, K.; Ouchi, T.; Huang, B.; Reichman, B.; Blankenship, R. Improvement in −40 ℃ electrochemical properties of AB_2 metal hydride alloy by silicon incorporation. *J. Alloy. Compd.* **2013**, *575*, 65–72.
98. Young, K.; Fetcenko, M.A.; Ouchi, T.; Li, F.; Koch, J. Effects of Sn-substitution in C14 Laves phase alloys for NiMH battery application. *J. Alloy. Compds* **2009**, *469*, 406–416.
99. Young, K.; Fetcenko, M.A.; Li, F.; Ouchi, T. Structural, thermodynamic, and electrochemical properties of $Ti_xZr_{1-x}(VNiCrMnCoAl)_2$ C14 Laves phase alloys. *J. Alloy. Compd.* **2008**, *464*, 238–247.
100. Young, K.; Fetcenko, M.A.; Li, F.; Ouchi, T.; Koch, J. Effect of vanadium substitution in C14 Laves phase alloys for NiMH battery application. *J. Alloy. Compd.* **2009**, *468*, 482–492.
101. Young, K.; Young, M.; Ouchi, T.; Reichman, B.; Fetcenko, M.A. Improvement in high-rate dischargeability, activation, and low-temperature performance in multi-phase AB_2 alloys by partial substitution of Zr by Y. *J. Power Sources* **2012**, *215*, 279–287.
102. Young, K.; Reichman, B.; Fetcenko, M.A. Electrochemical performance of AB_2 metal hydride alloys measured at −40 ℃. *J. Alloy. Compd.* **2013**. Available online: http://dx.doi.org/10.1016/j.jallcom.2013.01.125 (accessed on 18 June 2013).
103. Yasuoka, S.; Magari, Y.; Murata, T.; Tanaka, T.; Ishida, J.; Nakamura, H.; Nohma, T.; Kihara, M.; Baba, Y.; Teraoka, H. Development of high-capacity nickel-metal hydride batteries using superlattice hydrogen-absorbing alloys. *J. Power Sources* **2006**, *156*, 662–666.
104. Yasuoka, S.; Kihara, M. Development of high capacity nickel-metal hydride batteries using superlattice hydrogen-absorbing alloys. *Rare Earths* **2006**, *48*, 112–113.
105. Teraoka, H. Development of low self-discharge nickel-metal hydride battery. Available online http://www.scribd.com/doc/9704685/Teraoka-Article-En (accessed on 18 July 2013).
106. Ching, P.; Liu, S.; Tan, M. The research and development of A_2B_7-type of La_2Ni_7-based MH alloy. *Technol. Trend* **2011**, *14*, 23–24.
107. Zhang, Y.; Chen, L.; Yang, T.; Xu, C.; Ren, H.; Zhao, D. The electrochemical hydrogen storage performances of Si-added La-Mg-Ni-Co-based A_2B_7-type electrode alloys. *Rare Metals* **2013**. Available online; http://dx.doi.org/10.1007/s12598-013-0053-x (accessed on 21 June 2013).
108. Dong, Z.; Ma, L.; Ding, Y.; Wu, Y.; Shen, X.; Wang, L. Effects of sintering temperature on microstructure and electrochemical characteristics of La-Mg-Ni system hydrogen storage alloys. *J. Nanjing Univ. Technol.* **2011**, *33*, 12–15.
109. Liu, J.; Han, S.; Li, Y.; Yang, S.; Shen, W.; Zhang, L.; Zhou, Y. An investigation on phase transformation and electrochemical properties of as-cast and annealed $La_{0.75}Mg_{0.25}Ni_x$ (x = 3.0, 3.3, 3.5, 3.8) alloys. *J. Alloy. Compd.* **2013**, *552*, 119–126.
110. Hu, W.; Denys, R.V.; Nwakwuo, C.C.; Holm, T.; Maehlen, J.P.; Solberg, J.K.; Yartys, V.A. Annealing effect on phase composition and electrochemical properties of the Co-free La_2MgNi_9 anode for Ni-metal hydride batteries. *Electrochim. Acta* **2013**, *96*, 27–33.
111. Huang, T.; Yuan, X.; Yu, J.; Wu, Z.; Han, J.; Sun, G.; Xu, N.; Zhang, Y. Effects of annealing treatment and partial substitution of Cu for Co on phase composition and hydrogen storage performance of $La_{0.7}Mg_{0.3}Ni_{3.2}Co_{0.35}$ alloy. *Int. J. Hydrog. Energy* **2012**, *37*, 1074–1079.

112. Jiang, W.; Mo, X.; Wei, Y.; Zhou, Z.; Guo, J. Effect of annealing treatment on hydrogen storage properties of La-Ti-Mg-Ni-based alloy. *J. Rare Earths* **2012**, *30*, 450–455.
113. Jiang, W.; Qin, C.; Zhu, R.; Guo, J. Annealing effect on hydrogen storage property of Co-free $La_{1.8}Ti_{0.2}MgNi_{8.7}Al_{0.3}$ alloy. *J. Alloy. Compd.* **2013**, *565*, 37–43.
114. Fang, X.; Luo, Y.; Gao, Z.; Zhang, G.; Kang, L. Effects of annealing treatment on microstructure and electrochemical properties of $La_{0.68}Gd_{0.2}Mg_{0.12}Ni_{3.3}Co_{0.3}Al_{0.1}$ hydrogen storage alloys. *J. Funct. Mater.* **2012**, *20*, 2751–2756.
115. Guo, P.; Lin, Y.; Zhao, H.; Guo, S.; Zhao, D. Structure and high-temperature electrochemical properties of $La_{0.6}Nd_{0.15}Mg_{0.25}Ni_{3.3}Si_{0.10}$ hydrogen storage alloys. *J. Rare Earths* **2011**, *29*, 574–579.
116. Li, F.; Young, K.; Ouchi, T.; Fetcenko, M.A. Annealing effects on structural and electrochemical properties of $(LaPrNdZr)_{0.83}Mg_{0.17}(NiCoAlMn)_{3.3}$ alloy. *J. Alloy. Compd.* **2009**, *471*, 371–377.
117. Quao, Y.Q.; Zhao, M.S.; Zhang, Q.M.; Zhai, J. Crystal structure and some dynamic performances of $Ti_{0.25}V_{0.34}Du_{0.01}Cr_{0.1}Ni_{0.3}$ hydrogen storage electrode. *Chin. Chem. Lett.* **2011**, *22*, 93–96.
118. Luo, Y.; Feng, C.; Teng, X.; Kang, L. Study on electrochemical properties of annealed $R_{0.67}Mg_{0.33}Ni_{3.0}$ (*R* = La, Ce, Pr, Nd) hydrogen storage alloys. *Rare Metal. Mater. Eng.* **2010**, *39*, 90–95.
119. Zhou, X.; Young, K.; West, J.; Regalado, J.; Cherisol, K. Degradation mechanisms of high-energy bipolar nickel metal hydride battery with AB_5 and A_2B_7 alloys. *J. Alloy. Compd.* **2013**, in press.
120. Liu, Y.; Cao, Y.; Huang, L.; Gao, M.; Pan, H. Rare earth-Mg-Ni-based hydrogen storage alloys as negative electrode materials for Ni/MH batteries. *J. Alloy. Compd.* **2011**, *509*, 675–686.
121. Dong, Z.; Ma, L.; Wu, Y.; Wang, L.; Shen, X. Microstructure and electrochemical hydrogen storage characteristics of $(La_{0.7}Mg_{0.3})_{1-x}Ce_xNi_{2.8}Co_{0.5}$ (x = 0–0.20) electrode alloys. *Int. J. Hydrog. Energy* **2011**, *36*, 3016–3021.
122. Wang, B.; Chen, Y.; Liu, Y. Structure and electrochemical properties of $(La_{1-x}Dy_x)_{0.8}Mg_{0.2}Ni_{3.4}Al_{0.1}$ (x = 0.0–0.20) hydrogen storage alloys. *Int. J. Hydrog. Energy* **2012**, *37*, 9082–9087.
123. Luo, Y.; Jia, Q.; Wu, T.; Kang, L. Influence of rare-earth elements R on phase-structure and electrochemical properties of hydrogen storage alloys (LaRMg) $(NiCoAlZn)_{3.5}$. *J. Lanzhou Univ. Technol.* **2009**, *35*, 1–6.
124. Zhang, Y.; Hou, Z.; Li, B.; Ren, H.; Cai Y.; Zhao, D. Electrochemical hydrogen storage characteristics of as-cast and annealed $La_{0.8-x}Nd_xMg_{0.2}Ni_{3.15}Co_{0.2}Al_{0.1}Si_{0.05}$ (x = 0–0.4) alloys. *Trans. Nonferrous Metals Soc. China* **2013**, *23*, 1403–1412.
125. Liu, S.; Qin, M.; Qing, P.; Huang, X.; Huang, H.; Guo, J. Study on the hydrogen storage and electrochemical characteristics of $(La_{1-x}Nd_x)_2Mg(Ni_{0.8}Co_{0.15}Mn_{0.05})_9$ (x = 0~0.3) alloys. *Guangxi Sci.* **2011**, *18*, 242–245.
126. Ren, H.; Li, B.; Hou, Z.; Liu, X.; Chen, L.; Zhang, Y. Enhanced electrochemical cycle stability of RE-Mg-Ni system A_2B_7-type alloys by melt spinning and substituting La with Pr. *Adv. Mater. Res.* **2012**, *415–417*, 1603–1607.
127. Zhang, Y.; Hou, Z.; Yang, T.; Zhang, G.; Li, X.; Zhao, D. Structure and electrochemical hydrogen storage characteristics of $La_{0.8-x}Pr_xMg_{0.2}Ni_{3.15}Co_{0.2}Al_{0.1}Si_{0.05}$ (x = 0–0.4) electrode alloys. *J. Cent. South. Univ. Technol.* **2013**, *20*, 1142–1150.

128. Zhang, Y.; Cai, Y.; Zhao, C.; Zhai, T.; Zhang, G.; Zhao, D. Electrochemical performances of the as-melt $La_{0.75-x}M_xMg_{0.25}Ni_{3.2}Co_{0.2}Al_{0.1}$ (M = Pr, Zr; x = 0, 0.2) alloys applied to Ni/metal hydride (MH) battery. *Int. J. Hydrog. Energy* **2012**, *37*, 14590–14597.
129. Li, P.; Hou, Z.; Yang, T.; Shang, H.; Qu, X.; Zhang, Y. Structure and electrochemical hydrogen storage characteristics of the as-cast and annealed $La_{0.8-x}Sm_xMg_{0.2}Ni_{3.15}Co_{0.2}Al_{0.1}Si_{0.05}$ (x = 0–0.4) alloys. *J. Rare Earths* **2012**, *30*, 696–704.
130. Dong, Z.; Wu, Y.; Ma, L.; Shen, X.; Wang, L. Influences of low-Ti substitution for La and Mg on the electrochemical and kinetic characteristics of AB_3-type hydrogen storage alloy electrodes. *Sci. China Technol. Sci.* **2010**, *53*, 242–247.
131. Dong, Z.; Ma, L.; Wang, L.; Wu, Y.; Shen, X. Effects of substituting La with Ti on microstructure and electrochemical properties of AB_3-type hydrogen storage alloys. *J. Nanjing Univ. Technol.* **2011**, *33*, 57–62.
132. Zhang, Y.; Yang, T.; Shang, H.; Chen, L.; Ren, H.; Zhao, D. Electrochemical hydrogen storage kinetics of $La_{0.75-x}Zr_xMg_{0.25}Ni_{3.2}Co_{0.2}Al_{0.1}$ (x = 0–0.2) alloys prepared by melt spinning. *Energy Procedia* **2012**, *16*, 1275–1282.
133. Wei, F.; Li, Li.; Xiang, H.; Li, H.; Wei, F. Phase structure and electrochemical properties of $La_{1.7+x}Mg_{1.3-x}(NiCoMn)_{9.3}$ (x = 0 – 0.4) hydrogen storage alloys. *Trans. Nonferrous Metals Soc. China* **2012**, *22*, 1995–1999.
134. Jiang, L.; Lan, Z.; Li, G.; Guo, J. Influence of magnesium on electrochemical properties of $RE_{3-x}Mg_x(Ni_{0.7}Co_{0.2}Mn_{0.1})_9$ (x = 0.5–1.25) alloy electrodes. *J. Rare Earths* **2012**, *30*, 1255–1259.
135. Gao, Z.; Luo, Y.; Li, R.; Lin, Z.; Kang, L. Phase structures and electrochemical properties of $La_{0.8-x}Gd_{0.2}Mg_xNi_{3.1}Co_{0.3}Al_{0.1}$ hydrogen storage alloys. *J. Power Sources* **2013**, *241*, 509–516.
136. Gao, Z.; Kang, L.; Luo, Y. Influence of magnesium content on structure and performance of A_2B_7-type RE-Mg-Ni Hydrogen storage alloys. *Chem. J. Chin. Univ.* **2012**, *33*, 2035–2042.
137. Guo, X.; Luo, Y.; Gao, Z.; Zhang, G.; Kang, L. The effect of Mg on the microstructure and electrochemical properties of $La_{0.8-x}Gd_{0.2}Mg_xNi_{3.3}Co_{0.3}Al_{0.1}$ (x = 0–0.4) hydrogen storage alloys. *J. Funct. Mater.* **2012**, *18*, 2450–2455.
138. Dong, Z.; Wu, Y.; Ma, L.; Wang, L.; Shen, X.; Wang, L. Microstructure and electrochemical hydrogen storage characteristics of $La_{0.67}Mg_{0.33-x}Ca_xNi_{2.75}Co_{0.25}$ (x = 0–0.15) electrode alloys. *Int. J. Hydrog. Energy* **2011**, *36*, 3050–3055.
139. Dong, X.; Yang, L.; Li, X.; Wang, Q.; Ma, L.; Lin, Y. Effect of substitution of aluminum for nickel on electrochemical properties of $La_{0.75}Mg_{0.25}Ni_{3.5-x}Co_{0.2}Al_x$ hydrogen storage alloys. *J. Rare Earths* **2011**, *29*, 143–149.
140. Qin, M.; Liu, S.; Qing, P.; Lan, Z.; Guo, J. The influence of Co content on $LaNi_{3.2-x}Mn_{0.3}Co_x$ (x = 0.2~0.8) alloy hydrogen storage and electrochemical properties. *Phys. Procedia* **2011**, *22*, 577–583.
141. Lan, Z.; Yan, W.; Qin, C.; Lu, Z.; Jiang, J.; Guo, J. Preparation and electrochemical properties of $La_{0.7}Zr_{0.1}Mg_{0.2}Ni_{3.4-x}Co_xFe_{0.1}$ Alloy. *Guangxi Sci.* **2012**, *19*, 134–138.
142. Qin, M.; He, B.; Qing, P.; Lu, Z.; Liu, Y.; Guo, J. Effect of Co content on electrochemical properties of $La_{0.55}Pr_{0.05}Nd_{0.15}Mg_{0.25}Ni_{3.5-x}Co_xAl_{0.25}$ (x = 0~0.4) hydrogen storage alloy. *Mater. Sci. Eng. Powder Metall.* **2012**, *17*, 160–165.

143. Xiong, K.; Zhu, R.; Ding, Y.; Lan, Z.; Huang, C.; Guo, J. Study on the electrochemical properties of $La_{0.7}Mg_{0.3}Ni_{3.4-x}(Al_{0.3}Co_{0.4})_{0.2+x}$ (x = 0~0.3) hydrogen storage alloy electrodes. *Guangxi Sci.* **2012**, *19*, 57–63.
144. Dong, Z.; Ma, L.; Shen, X.; Wang, L.; Wu, Y.; Wang, L. Cooperative effect of Co and Al on the microstructure and electrochemical properties of AB_3-type hydrogen storage electrode alloys for advanced MH/Ni secondary battery. *Int. J. Hydrog. Energy* **2011**, *36*, 893–900.
145. Qin, M.; Lan, Z.; Ding, Y.; Xiong, K.; Liu, Y.; Guo, J. A study on hydrogen storage and electrochemical properties of $La_{0.55}Pr_{0.05}Nd_{0.15}Mg_{0.25}Ni_{3.5}(Co_{0.5}Al_{0.5})_x$ (x = 0.0, 0.1, 0.3, 0.5) alloys. *J. Rare Earths* **2012**, *30*, 222–227.
146. Wang, W.; Chen, Y.; Li, Q.; Yang, W. Microstructures and electrochemical properties of $LaNi_{3.8-x}Al_x$ hydrogen storage alloys. *J. Rare Earths* **2013**, *31*, 497–501.
147. Qin, M.; Liu, S.; Qing, P.; Lan, Z.; Guo, J. Effect of Mn substitution for Ni on hydrogen storage properties and electrochemical characteristics of $(La_{0.8}Nd_{0.2})_2Mg(Ni_{0.9-x}Co_{0.1}Mn_x)_9$ alloys. *Mater. Rev.* **2011**, *25*, 35–39.
148. Zhang, H.; Wang, B.; Wang, D.; Sui, Y.; He, D.; Xia, B. Effect of Mn content on the structure and electrochemical characteristics of $(La_{0.78}Mg_{0.22})(Ni_{(0.9-x)}Co_{0.1}Mn_x)_{3.5}$ hydrogen storage alloys. *Shanghai Metals* **2010**, *32*, 16–19.
149. Pavlyuk, V.; Pozycka-Sokolowska, E.; Marciniak, B.; Paul-Boncour, V.; Dorogova, M. The structural, magnetic, hydrogenation and electrode properties of $REMg_2Cu_{9-x}Ni_x$ alloys (RE = La, Pr, Tb). *Cent. Eur. J. Chem.* **2011**, *9*, 1133–1142.
150. Hou, C.; Zhao, M.; Li, J.; Huang, L. Phase structure and electrochemical characteristics of $CeMn_{0.25}Al_{0.25}Ni_{1.5+x}$ (x = 0.0, 0.3, 0.5, 0.7, 0.9, 1.1) alloys. *Rare Metal. Mater. Eng.* **2012**, *41*, 100–104.
151. Young, K.; Wu, A.; Qiu, Z.; Tan, J.; Mays, W. Effects of H_2O_2 addition to the cell balance and self-discharge of Ni/MH batteries with AB_5 and A_2B_7 alloys. *Int. J. Hydrog. Energy* **2012**, *37*, 9882–9891.
152. Nwakwuo, C.C.; Holm, T.; Denys, R.V.; Hu, W.; Maehlen, J.P.; Solberg, J.K.; Yartys, V.A. Effect of magnesium content and quenching rate on the phase structure and composition of rapidly solidified La_2MgNi_9 metal hydride battery electrode alloy. *J. Alloy. Compd.* **2013**, *555*, 201–208.
153. Tang, C.; Pan, W.; Qin, Y.; Zhou, H. Preparation and hydrogen storage properties of $La_{0.7}Mg_{0.3}Ni_{2.8}Co_{0.5-x}Fe_x$ series alloys. *Chin. J. Nonferrous Metals* **2011**, *21*, 1373–1379.
154. Yang, S.; Liu, H.; Han, S.; Li, Y.; Shen, W. Effects of electrodeless composite plating Ni-Cu-P on the electrochemical properties of La-Mg-Ni-based hydrogen storage alloy. *Appl. Surf. Sci.* **2013**, *271*, 210–215.
155. Zhang, J.; Villeroy, B.; Knosp, B.; Bernard, P.; Latroche, M. Structural and chemical analyses of the new ternary La_5MgNi_{24} phase synthesized by spark plasma sintering and used as negative electrode material for Ni-MH batteries. *Int. J. Hydrog. Energy* **2012**, *37*, 5225–5233.
156. Shen, W.; Han, S.; Li, Y.; Yang, S.; Miao, Q. Effect of electroplating polyaniline on electrochemical kinetics of La-Mg-Ni-based hydrogen storage alloy. *Appl. Surf. Sci.* **2012**, *258*, 6316–6320.
157. Yang, Z.P.; Li, Q.; Zhao, X.J. Influence of magnetic annealing on electrochemical performance of $La_{0.67}Mg_{0.33}Ni_{3.0}$ hydride electrode alloy. *J. Alloy. Compd.* **2013**, *558*, 99–104.

158. Zhang, S.; Wang, D.; Hou, X.; Huang, X.; Sun, L. Research on a new synthesis technology of La-Mg-Ni system alloys and microstructure of $La_{0.67}Mg_{0.33}Ni_{3.0}$ alloys. *Rare Metal. Mater. Eng.* **2012**, *41*, 2075–2080.
159. Justi, E.W.; Ewe, H.H.; Kalberlah, A.W.; Saridakis, N.M.; Schaefer, M.H. Electrocatalysis in the nickel-titanium system. *Energy Convers.* **1970**, *10*, 146–156.
160. Gutjahr, M.A.; Buchner, H.; Beccu, K.D.; Saeufferer, H. A new type of reversible negative electrode for alkaline storage batteries based on metal alloy hydrides. *Power Sources* **1973**, *4*, 79–91.
161. Beccu, K. Negative electrode of titanium-nickel alloy hydride phases. U.S. Patent 3,824,131, 16 July 1974.
162. Zhao, X.; Li, J.; Yao, Y.; Ma, L.; Shen, X. Electrochemical hydrogen storage properties of non-equilibrium Ti_2Ni alloy. *RSC Adv.* **2012**, *2*, 2149–2153.
163. Emami, H.; Cuevas, F. Hydrogenation properties of shape memory Ti(Ni, Pd) compds. *Intermetallics* **2011**, *19*, 876–886.
164. Emami, H.; Souques, R.; Crivello, J.; Cuevas, F. Electronic and structural influence of Ni by Pd substitution on the hydrogenation properties of TiNi. *J. Solid State Chem.* **2013**, *198*, 475–484.
165. Nei, J.; Young, K.; Wong, D.F. Electrochemical properties of $TiNi_{0.9}X_{0.1}$ (X = Ni, Cr, Mn, Fe, Co, Cu) metal hydride alloys. *J. Alloy. Compd.* Being prepared for submission.
166. Zhao, X.; Ma, L.; Qu, X.; Ding, Y.; Shen, X. Effect of mechanical milling on the structure and electrochemical properties of Ti_2Ni alloy in an alkaline battery. *Energy Fuels* **2009**, *23*, 4678–4682.
167. Zhao, X.; Ma, L.; Yao, Y.; Ding, Y.; Shen, X. Ti_2Ni alloy: A potential candidate for hydrogen storage in nickel/metal hydride secondary batteries. *Energy Environ. Sci.* **2010**, *3*, 1316–1321.
168. Zhao, X.; Zhou, J.; Shen, X.; Yang, M.; Ma, L. Structure and electrochemical hydrogen storage properties of A_2B-type Ti-Zr-Ni alloys. *Int. J. Hydrog. Energy* **2012**, *37*, 5050–5055.
169. Li, X.D.; Elkedim, O.; Nowak, M.; Jurczyk, M.; Chassagnon, R. Structural characterization and electrochemical hydrogen storage properties of $Ti_{2-x}Zr_xNi$ (x = 0, 0.1, 0.2) alloys prepared by mechanical alloying. *Int. J. Hydrog. Energy* **2013**, *38*, 12126–12132.
170. Cao, X.; Ma, L.; Yang, M.; Zhao, X.; Ding, Y. Electrochemical properties of the amorphous Ti_3Ni_2 alloy in Ni/MH batteries. *Rare Metal. Mater. Eng.* **2012**, *41*, 1511–1515.
171. Gibbons, P.C.; Kelton, K.F. *Physical Properties of Quasicrystals*; Stadnik, Z.M., Ed.; Springer: Berlin, Germany, 1999; p. 403.
172. Takasaki, A.; Kuroda, C.; Lee, S.; Kim, J. Electrochemical properties of $Ti_{45}Zr_{38-x}Ni_{17+x}$ ($0 \leq x \leq 8$) quasicrystals produced by rapid-quenching. *J. Alloy. Compd.* **2011**, *509*, S782–S785.
173. Baster, D.; Takasaki, A.; Kuroda, C.; Hanc, E.; Lee, S.; Swierczek, K.; Szmyd, J.S.; Kim, J.; Molenda, J. Effect of mechanical milling on electrochemical properties of $Ti_{45}Zr_{38-x}Ni_{17+x}$ (x = 0, 8) quasicrystals produced by rapid-quenching. *J. Alloy. Compd.* **2003**. Available online: http://dx.doi.org/10.1016/j.jallcom.2013.03.272 (accessed on 27 May 2013).
174. Ariga, Y.; Takasaki, A.; Kuroda, C.; Kulka, A. Electrochemical properties of $Ti_{45-x}Zr_{30+x}Ni_{25}$ (x = −4, 0, 4) quasicrystal and amorphous electrodes produced by mechanical alloying. *J. Alloy. Compd.* **2003**, in press.
175. Hu, W.; Wang, L.; Wang, L. Quinary icosahedral qausicrystalline Ti-V-Ni-Mn-Cr alloy: A novel anode material for Ni-MH rechargeable batteries. *Mater. Lett.* **2011**, *65*, 2868–2871.

176. Hu, W.; Yi, J.; Zheng, B.; Wang, L. Icosahedral qausicrystalline $(Ti_{1.6}V_{0.4}Ni)_{100-x}Sc_x$ alloys: Synthesis, structure and their application in Ni-MH batteries. *J. Solid State Chem.* **2013**, *202*, 1–5.
177. Ma, F.; Liu, X.; Yan, S.; Ao, D.; Ren, Y. Research progress of influence factors on electrochemical performance of Mg-base hydrogen storage alloys. *Metallic Funct. Mater.* **2011**, *34*, 67–70.
178. Anik, M.; Özdemir. G.; Küçükdeveci, N.; Baksan, B. Effect of Al, B, Ti and Zr additive elements on the electrochemical hydrogen storage performance of MgNi alloy. *Int. J. Hydrog. Energy* **2011**, *36*, 1568–1577.
179. Anik, M.; Özdemir, G.; Küçükdeveci, N. Electrochemical hydrogen storage characteristics of Mg-Pd-Ni ternary alloys. *Int. J. Hydrog. Energy* **2011**, *36*, 6744–6750.
180. Anik, M. Effect of titanium additive element on the discharging behavior of MgNi alloy electrode. *Int. J. Hydrog. Energy* **2011**, *36*, 15075–15080.
181. Anik, M.; Karanfil, F.; Küçükdeveci, N. Development of the high performance magnesium based hydrogen storage alloy. *Int. J. Hydrog. Energy* **2012**, *37*, 299–308.
182. Etiemble, A.; Idrissi, H. On the decrepitation mechanism of MgNi and $LaNi_5$-based electrodes studied by *in situ* acoustic emission. *J. Power Sources* **2011**, *196*, 5168–5173.
183. Etiemble, A.; Idrissi, H.; Roué, L. *In situ* investigation of the volume change and pulverization of hydride materials for Ni-MH batteries by concomitant generated force and acoustic emission measurements. *J. Power Sources* **2012**, *205*, 500–505.
184. Kim, S.; Chourashiya, M.G.; Park, C.; Park, C. Electrochemical performance of NAFION coated electrodes of hydriding combustion synthesized MgNi based composite hydride. *Mater. Lett.* **2013**, *93*, 81–84.
185. Liu, J. Effect of Ti-La substitution on electrochemical properties of amorphous MgNi-based secondary hydride electrodes. *J. Tianjin Norm. Univ.* **2011**, *31*, 67–70.
186. Etiemble, A.; Idrissi, H. Effect of Ti and Al on the pulverization resistance of MgNi-based metal hydride electrodes evaluated by acoustic emission. *Int. J. Hydrog. Energy* **2013**, *38*, 1136–1144.
187. Etiemble, A.; Rouosselot, S.; Guo, W.; Idrissi, H.; Roué, L. Influence of Pd addition on the electrochemical performance of Mg-Ni-Ti-Al-based metal hydride for Ni-MH batteries. *Int. J. Hydrog. Energy* **2013**, *38*, 7169–7177.
188. Santos, S.F.; de Castro, J.F.R.; Ticianelli, E.A. Microstructures and electrode performances of $Mg_{50}Ni_{(50-x)}Pd_x$ alloys. *Cent. Eur. J. Chem.* **2013**, *11*, 485–491.
189. Spassov, T.; Köster, U. Thermal stability and hydriding properties of nanocrystalline melt-spun $Mg_{63}Ni_{30}Y_7$. *J. Alloy. Compd.* **1998**, *279*, 279–286.
190. Zhang, Y.; Song, C.; Ren, H.; Li, Z.; Hu, F.; Zhao, D. Enhanced hydrogen storage kinetics of nanocrystalline and amorphous Mg_2N-type alloy by substituting Ni with Co. *Trans. Nonferrous Metals Soc. China* **2011**, *21*, 2002–2009.
191. Zhang, Y.; Zhao, D.; Ren, H.; Guo, S.; Qi, Y.; Wang, X. Enhanced electrochemical hydrogen storage characteristics of nanocrystalline and amorphous $Mg_{20}Ni_{10-x}Co_x$ (x = 0–4) alloys by melt spinning. *Rare Metal. Mater. Eng.* **2011**, *40*, 1146–1151.

192. Zhang, Y.; LU, K.; Zhao, D.; Guo, S.; Qi, Y.; Wang, X.; Electrochemical hydrogen storage characteristics of nanocrystalline and amorphous Mg_2Ni-type alloys prepared by melt-spinning. *Trans. Nonferrous Metals Soc. China* **2011**, *21*, 502–511.
193. Zhang, Y.; Zhang, G.; Yang, T.; Hou, Z.; Guo, S.; Qi, Y.; Zhao, D. Electrochemical and hydrogen absorption/desorption properties of nanocrystalline Mg_2Ni-type alloys prepared by melt spinning. *Rare Metal. Mater. Eng.* **2012**, *41*, 2069–2074.
194. Zhang, Y.; Yang, T.; Shang, H.; Zhao, C.; Xu, C.; Zhao, D. The electrochemical hydrogen storage characteristics of as-spun nanocrystalline and amorphous $Mg_{20}Ni_{10-x}M_x$ (M = Cu, Co, Mn; x = 0–4) alloys. *Rare Metals* **2013**. Available online: http://dx.doi.org/10.1007/s12598-013-0051-z (accessed on 15 July 2013).
195. Zhang, Y.; Zhao, C.; Yang, T.; Shang, H.; Xu, C.; Zhao, D. Comparative study of electrochemical performances of the as-melt $Mg_{20}Ni_{10-x}M_x$ (M = None, Cu, Co, Mn; x = 0, 4) alloys applied to Ni/metal hydride (MH) battery. *J. Alloy. Compd.* **2013**, *555*, 131–137.
196. Zhang, Y.; Qi, Y.; Zhao, D.; Guo, S.; Ma, Z.; Wang, X. An investigation of hydrogen storage kinetics of melt-spun nanocrystalline and amorphous Mg_2Ni-type alloys. *J. Rare Earths* **2011**, *29*, 87–93.
197. Zhang, Y.; Li, B.; Ren, H.; Hou, Z.; Hu, F.; Wang, X. Influences of melt spinning on electrochemical hydrogen storage performance of nanocrystalline and amorphous Mg_2Ni-type alloys. *J. Cent. South. Univ. Technol.* **2011**, *18*, 1825–1832.
198. Huang, L.W.; Elkedim, O.; Nowak, M.; Chassagnon, R.; Jurczyk, M. $Mg_{2-x}Ti_xNi$ (x = 0, 0.5) alloys prepared by mechanical alloying for electrochemical hydrogen storage: Experiments and first-principles calculations. *Int. J. Hydrog. Energy* **2012**, *37*, 14248–14256.
199. Zhang, J.; Zhu, Y.; Wang, Y.; Pu, Z.; Li, L. Electrochemical hydrogen storage properties of $Mg_{2-x}Al_xNi$ (x = 0, 0.3, 0.5, 0.7) prepared by hydriding combustion synthesis and mechanical milling. *Int. J. Hydrog. Energy* **2012**, *37*, 18140–18147.
200. Jiang, C.; Wang, H.; Wang, Y.; Cheng, X.; Tang, Y.; Liu, Z.; Xie, H. Enhanced electrochemical performance of Mg_2Ni alloy prepared by rapid quenching in magnetic field. *J. Power Sources* **2013**, *238*, 257–264.
201. Zhu, Y.; Yang, C.; Zhu, J.; Li, L. Structural and electrochemical hydrogen storage properties of Mg_2Ni-based alloys. *J. Alloy. Compd.* **2011**, *509*, 5309–5314.
202. Rousselot, S.; Guay, D.; Roue, L. Comparative study on the structure and electrochemical hydriding properties of MgTi, $Mg_{0.5}Ni_{0.5}Ti$ and $MgTi_{0.5}Ni_{0.5}$ alloys prepared by high energy ball milling. *J. Power Sources* **2011**, *196*, 1561–1568.
203. Cao, Z.; Wu, D.; Li, C.; Bian, J.; Zhang, K. Effect of Ni addition on electrochemical properties of Mg-Al hydrogen storage alloy. *J. Shenyang Norm. Univ.* **2013**, *31*, 16–20.
204. Yang, C.; Zhu, Y.; Zhang, W.; Zhu, J.; Li, L. Effects of metal doping on electrochemical properties of Mg-based hydrogen storage alloys. *J. Nanjing Univ. Technol.* **2011**, *33*, 52–57.
205. Anik, M. Improvement of the electrochemical hydrogen storage performance of magnesium based alloys by various additive elements. *Int. J. Hydrog. Energy* **2012**, *37*, 1905–1911.
206. Huang, L.W.; Elkedim, O.; Nowak, M.; Jurczyk, M.; Cahssagnon, R.; Meng, D.W. Synergistic effects of multiwalled carbon nanotubes and Al on the electrochemical hydrogen storage

properties of Mg_2Ni-type alloy prepared by mechanical alloying. *Int. J. Hydrog. Energy* **2012**, *37*, 1538–1545.

207. Xu, J.; Niu, D.; Fan, Y. Electrochemical hydrogen storage performance of $Mg_{2-x}Al_xNi$ thin films. *J. Power Sources* **2012**, *198*, 383–388.
208. Akiba, E.; Iba, H. Hydrogen absorption by Lases phase related BCC solid solution. *Intermetallics* **1998**, *6*, 461–470.
209. Chai, Y.J.; Zhao, M.S.; Wang, N. Crystal structural and electrochemical properties of $Ti_{0.15}Zr_{0.08}V_{0.35}Cr_{0.10}Ni_{0.30-x}Mn_x$ (x = 0–0.12) alloys. *Mater. Sci. Eng. B* **2008**, *147*, 47–51.
210. Guéguen, A.; Joubert, J.M.; Latroche, M. Influence of the C14 $Ti_{35.4}V_{32.3}Fe_{32.3}$ Laves phase on the hydrogenation properties of the body-centered cubic compd $Ti_{24.5}V_{59.3}Fe_{16.2}$. *J. Alloy. Compd.* **2011**, *509*, 3013–3018.
211. Wang, N.; Chai, Y. Electrochemical properties and reaction mechanism of Ti-V multiphase alloy at high temperature. *Rare Metal. Mater. Eng.* **2011**, *40*, 1519–1521.
212. Wang, Y.; Zhao, M. Electrochemical hydrogen storage characteristics of $Ti_{0.10}Zr_{0.15}V_{0.35}Cr_{0.10}Ni_{0.30}$ − 10% $LaNi_3$ composite and its synergetic effect. *Trans. Nonferrous Metals Soc. China* **2012**, *22*, 2000–2006.
213. Wang, Y.; Zhao, M. Distinct synergistic effect in $Ti_{0.10}Zr_{0.15}V_{0.35}Cr_{0.10}Ni_{0.30}$ + 1.0 wt % $LaNi_5$ hydrogen storage composite electrode. *Int. J. Hydrog. Energy* **2012**, *37*, 3276–3282.
214. Wang, Y.; Zhao, M. Electrochemical characteristics and synergetic effect of $Ti_{0.10}Zr_{0.15}V_{0.35}Cr_{0.10}Ni_{0.30}$ − 10 wt % $LaNi_5$ hydrogen storage composite electrode. *J. Rare Earths* **2012**, *30*, 146–150.
215. Inoue, H.; Koyama, S.; Higuchi, E. Charge-discharge performance of Cr-substituted V-based hydrogen storage alloy negative electrodes for use in nickel-metal hydride batteries. *Electrochim.Acta* **2012**, *59*, 23–31.
216. Hang, Z.; Xiao, X.; Li, S.; Ge, H.; Chen, C.; Chen, L. Influence of heat treatment on the microstructure and hydrogen storage properties of $Ti_{10}V_{77}Cr_6Fe_6Zr$ alloy. *J. Alloy. Compd.* **2012**, *529*, 128–133.
217. Liu, W.; Wang, X.; Hu, W.; Kawabe, Y.; Watada, M.; Wang, L. Electrochemical performance of TiVNi-Quasicrystal and AB_3-Type hydrogen storage alloy composite materials. *Int. J. Hydrog. Energy* **2011**, *36*, 616–620.
218. Liu, W.; Zhang, S.; Wang, L. $Ti_{1.4}V_{0.6}Ni$ quasicrystal and its composites with $x V_{18}Ti_{15}Zr_{18}Ni_{29}Cr_5Co_7Mn$ alloy used as negative electrode materials for the nickel-metal hydride (Ni-MH) secondary batteries. *Mater. Lett.* **2012**, *79*, 122–124.
219. Liu, W.; Zhang, S.; Wang, L. Influence of heat treatment on electrochemical properties of $Ti_{1.4}V_{0.6}Ni$ alloy electrode containing icosahedral quasicrystalline phase. *Trans. Nonferrous Metals Soc. China* **2012**, *22*, 3034–3038.
220. Liu, W.; Liang, F.; Zhang, S.; Lin, J.; Wang, X.; Wang, L. Electrochemical properties of Ti-based Quasicrystal and ZrV_2 Laves phase alloy composite materials as negative electrode for Ni-MH secondly batteries. *J. Non-Cryst. Solids* **2012**, *358*, 1846–1849.
221. Liu, W.; Kawabe, Y.; Liang, F.; Okuyama, R.; Lin, J.; Wang, L. A composite based on Fe substituted TiVNi alloy: Synthesis, structure and electrochemical hydrogen storage property. *Intermetallics* **2013**, *34*, 18–22.

222. Young, K.; Ouchi, T.; Fetcenko, M.A.; Mays, W.; Reichman, B. Structural and electrochemical properties of $Ti_{1.5}Zr_{5.5}V_xNi_{10-x}$. *Int. J. Hydrog. Energy* **2009**, *34*, 8695–8706.
223. Young, K.; Ouchi, T.; Huang, B.; Nei, J.; Fetcenko, M.A. Studies of $Ti_{1.5}Zr_{5.5}V_{0.5}(M_xNi_{1-x})_{9.5}$ (M = Cr, Mn, Fe, Co, Cu, Al): Part 1. Structural characteristics. *J. Alloy. Compd.* **2010**, *501*, 236–244.
224. Young, K.; Nei, J.; Huang, B.; Ouchi, T.; Fetcenko, M.A. Studies of $Ti_{1.5}Zr_{5.5}V_{0.5}(M_xNi_{1-x})_{9.5}$ (M = Cr, Mn, Fe, Co, Cu, Al): Part 2. Hydrogen storage and electrochemical properties. *J. Alloy. Compd.* **2010**, *501*, 245–254.
225. Nei, J.; Young, K.; Salley, S.O.; Ng, K.Y.S. Effects of annealing to $Zr_8Ni_{19}X_2$ (*X* = Ni, Mg, Al, Sc, V, Mn, Co, Sn, La, and Hf): Structural characteristics. *J. Alloy. Compd.* **2012**, *516*, 144–152.
226. Nei, J.; Young, K.; Salley, S.O.; Ng, K.Y.S. Effects of annealing on $Zr_8Ni_{19}X_2$ (*X* = Ni, Mg, Al, Sc, V, Mn, Co, Sn, La, and Hf): Hydrogen storage and electrochemical properties. *Int. J. Hydrog. Energy* **2012**, *37*, 8418–8427.
227. Lee, H.; Chourashiya, M.G.; Park, C.; Park, C. Hydrogen storage and electrochemical properties of the $Ti_{0.32}Cr_{0.43-x-y}V_{0.25}Fe_xMn_y$ (x = 0–0.055, y = 0–0.080) alloys and their composites with $MmNi_{3.99}Al_{0.29}Mn_{0.3}Co_{0.6}$ alloy. *J. Alloy. Compd.* **2013**, *566*, 37–42.
228. Huang, H.; Huang, K. Effect of AB_5 alloy on electrochemical properties of $Mm_{0.80}Mg_{0.20}Ni_{2.56}Co_{0.50}Mn_{0.14}Al_{0.12}$ hydrogen storage alloy. *Powder Technol.* **2012**, *221*, 365–370.
229. Huang, H.; Huang, K.; Chen, D.; Liu, S.; Zhuang, S. The electrochemical properties of MgNi-*x* wt % $TiNi_{0.56}Co_{0.44}$ (x = 0, 10, 30, 50) composite alloys. *J. Mater. Sci.* **2010**, *45*, 1123–1129.
230. Zlatanova, Z.; Spassov, T.; Eggeler, G.; Spassova, M. Synthesis and hydriding/dehydring properties of Mg_2Ni-AB (AB = TiNi or TiFe) nanocomposites. *Int. J. Hydrog. Energy* **2011**, *36*, 7559–7566.
231. Hsu, F.; Lin, C.; Lee, S.; Lin, C.; Bor, H. Effect of Mg_3MnNi_2 on the electrochemical characteristics of Mg_2Ni electrode alloy. *J. Power Sources* **2010**, *195*, 374–379.
232. Lee, S.; Hsu, F.; Chen, W.; Lin, C.; Lin, J. Influence of Mg_3AlNi_2 content on the cycling stability of Mg_2Ni-Mg_3AlNi_2 hydrogen storage alloy electrodes. *Intermetallics* **2011**, *19*, 1953–1958.
233. Lee, S.; Huang, C.; Chou, Y.; Hsu, F. Horng, J. Effects of Co and Ti on the electrode properties of Mg_3MnNi_2 alloy by ball-milling process. *Intermtallics* **2013**, *34*, 122–127.
234. He, W.; Zhao, Y.; Huang, J.; Zhang, Y.; Zeng, L. Electrochemical performance of compds $Ho_6Fe_{23-x}Co_x$ (x = 0, 1, 3). *J. Rare Earths* **2011**, *29*, 124–128.
235. Yao, X.; Ma, R.; Huang, J.; He, J.; He, W.; Zeng, L. Electrochemical performance of Gd-Co-Mn alloys. *J. Rare Earths* **2012**, *30*, 540–544.